Power Distance Table for EV Charger Stations in Distribution System

Iman Babaeiyazdi

A THESIS SUBMITTED TO
THE FACULTY OF GRADUATE STUDIES
IN PARTIAL FULFILLMENT OF THE REQUIREMENTS
FOR THE DEGREE OF
MASTER OF APPLIED SCIENCE

GRADUATE PROGRAM IN
ELECTRICAL ENGINEERING AND COMPUTER SCIENCE

YORK UNIVERSITY

TORONTO, ONTARIO

August 2019

Abstract

In this thesis, the aim is to investigate the unbalanced voltage behaviour of the fast charging stations and their effects on distribution power systems. In the first stage, the fast charger is developed to derive the response of the charger to the unbalanced input voltage. This response allows us to model the charging station as a load in power flow analysis. In the next stage of the study, a simplified model is proposed to incorporate the behaviour of the fast charger in power flow analysis. Different feeders data of IEEE benchmarks such as IEEE 34-bus, 37-bus, and 123-bus are used in the base benchmark, which is IEEE 30-bus, using the proposed simplified model. Then, maximum charging capacity of the stations and unbalanced voltage ratio (UVR) is calculated for any bus of interest that the charging station has been connected to. This task is done while the system is exposed to two constraints of UVR and voltage. The power flow analysis results indicate that for the different feeders' data, UVR of the system after connection of charging stations is the dominant constraint for some buses and it prevents further integration of fast charging station to the distribution system. Therefore, in order to mitigate unbalanced voltage in the system, partial transposition is utilized. In the partial transposition, the feeders are transposed and divided in two equal sections. After applying partial transposition to the feeders data, for the case of IEEE 34-bus, the UVR after connection of charging station was below the permissible value of 3%, but for IEEE 37-bus and 123-bus some buses still suffer from high UVR. Accordingly, a modified partial transposition was adopted as another alternative. The results demonstrate that the UVR of the system after applying modified partial transposition to the feeder data of IEEE 37-bus and 123-bus has decreased below the standard value of 3% and the system can accommodate higher capacity of fast charging stations. Finally, according to the power flow analysis a power distance table is acquired for the feeders' data that predicts the maximum charging capacity that can be connected to the system based on its distance from the main source without violating the system's operational constraint.

Acknowledgments

I would like to express my truthful gratitude to my supervisor Dr. Afshin Rezaei-Zare for his dedication to help me. His advice helped me to pass the obstacles I had confronted and accomplish this part of my life.

I also would like to thank my beloved parents for their continuous encouragement through my whole life. To those who indirectly contributed in this research, your kindness means a lot to me. Thank you very much.

I would like to thank Dr. John Lam and Dr. Solomon Boakye-Yiadom for helping to enhance my thesis with their valuable comments.

Finally, I appreciate my friend's encouragement and support during these two years for completing this task.

Contents

Abstract ii
Acknowledgments iii
Contents iv
List of Tables vi
List of Figures vii
Abbreviation ix
Chapter 1 1
1.1 Introduction 1
1.2 Thesis Overview 7
Chapter 2 Review of PEVs' Chargers 9
2.1 Chargers' Infrastructure 9
2.2 Charging stations 10
2.2.1 Level 1 Charging 10
2.2.2 Level 2 Charging 10
2.2.3 Level 3 Charging 11
2.3 International Standards and Charging Codes for EVs 13
2.3.1 Society for Automotive Engineers (SAE) 13
2.3.2 International Energy Agency 13
2.3.3 Deutsches Institut Fur Normung 13
2.3.4 International Electrotechnical Commission (IEC) 13
2.3.5 Institute of Electrical and Electronic Engineers (IEEE) 13
2.3.6 Infrastructure Working Council (IWC) 14
2.3.7 National Fire Protection Association (NFPA) 14
2.4 Charger Topology 14
2.4.1 Unidirectional Charger 15
2.4.2 Bidirectional Charger 15
2.5 Charging Methods 16
2.5.1 Constant Current 16
2.5.2 Constant Voltage 17
2.5.3 Constant Current- Constant Voltage 17

2.5.4 Pulse Current 17
2.5.5 Multistage Constant Current 17
2.6 Charger Simulation 20
2.6.1 AC/DC Converter Design 20
2.6.2 DC/DC Converter Design 24
2.7 Simulation results 26
2.7.1 First Scenario: Charger Operation under Normal Condition 26
2.7.2 Second Scenario: Charger Operation under Unbalanced Condition 30
Chapter 3 Power Flow Analysis of Studied System 36
3.1 Introduction 36
3.2 Power Flow Solution 36
3.2.1 Bus Admittance Matrix 37
3.2.2 Newton-Raphson Power Flow Solution For a typical bus of the power system which has been shown in Figure 3.2 current equation using KCL can be expressed in (3.10). 39
3.2.3 Studied System Data 42
3.2.4 Investigation of System Behaviour with Unbalanced Feeders 48
Chapter 4 Mitigation Method 62
4.1 Introduction 62
4.2 Line Transposition 64
4.3 Methodology 67
4.3.1 Partial transposition 67
4.3.2 Modified Partial Transposition 72
4.4 Power Distance Table 75
Chapter 5 Contributions and Future works 78
5.1 Contributions and conclusions 78
5.2 Future works 80
References 83
Appendix A Symmetrical Components A-1
A.1 Fundamentals of Symmetrical Components A-1
Appendix B B-5
B.1 Newton-Raphson Algorithm B-5

List of Tables

Table 2.1 – Types of charging power levels [1]. 12
Table 2.2 – Power system and AC/DC converter parameters [46], [47]. 22
Table 2.3 –DC/DC converter parameters. 24
Table 3.1 –Bus data for IEEE 30-bus benchmark. 43
Table 3.2 – Line data for IEEE 30-bus benchmark. 44
Table 3.3 –Voltage magnitude and phase angle of buses. 46
Table 3.4 – Overhead line spacing. 51
Table 3.5 – Conductor Data. 53
Table 3.6 –Cable spacing. 53
Table 3.7 – Neutral 15 kV All Aluminum (AA) Cable. 54
Table 3.8 – IEEE 34-bus feeder data (Configuration 300). 55
Table 3.9 – IEEE 37-bus feeder data (Configuration 721). 58
Table 3.10 – IEEE 123-bus feeder data (Configuration 1). 60
Table 4.1 – Power distance table. 75

List of Figures

Figure 1.1– Thesis overview. 8
Figure 2.1– Generic schematic of a PEV charger with onboard and off board configurations. 10
Figure 2.2– Single phase unidirectional resonant charger. 15
Figure 2.3– Single phase bidirectional resonant charger. 16
Figure 2.4– Charging methods. (a) CC-CV. (b) Pulse Current. (c) MSCC. 19
Figure 2.5– Simulated fast charger schematic. 20
Figure 2.6– Power factor correction control system. 21
Figure 2.7– Voltage waveform of converter's switch. 23
Figure 2.8– Flowchart of CC-CV charging method. 25
Figure 2.9– CC-CV charging controller. 26
Figure 2.10– Phase input voltage and current of the charger. (a) During the whole simulation. (b) Zoomed-in during CC mode. (c) during CV mode 28
Figure 2.11– THD of input current (phase A). 29
Figure 2.12– DC link voltage of AC/DC converter. 29
Figure 2.13– Voltage and current of battery. 29
Figure 2.14– UVR percentage applied to the charger 30
Figure 2.15– Three phase input voltage of the charger after applying negative sequence voltage. 31
Figure 2.16– Input voltage and current of phase A after applying negative sequence voltage. 32
Figure 2.17– THD of input current after applying negative sequence voltage (Phase A). 32
Figure 2.18– DC link voltage of AC/DC converter after applying negative sequence voltage. 33
Figure 2.19– Voltage and current of the battery after applying negative sequence voltage. 33
Figure 2.20– UCR of input current after applying negative sequence voltage in terms of time. 34
Figure 2.21– UCR of input current after applying negative sequence voltage in terms of UVR. 34
Figure 3.1– A simple circuit. 37
Figure 3.2– Typical bus of the power system [54]. 39
Figure 3.3– One line diagram of IEEE 30-bus benchmark [55]. 43

Figure 3.4– Simplified proposed model.....49
Figure 3.5– Overhead line spacing [56].....52
Figure 3.6–Cable spacing [56].....54
Figure 3.7– BUVR of system buses.....56
Figure 3.8– Maximum fast charging capacity. 57
Figure 3.9– UVR after connection of fast charging station. 57
Figure 3.10– BUVR of system buses.....58
Figure 3.11– Maximum charging station capacity. 59
Figure 3.12– UVR after connection of charging station.....59
Figure 3.13– BUVR of system's buses.....60
Figure 3.14– Maximum charging station capacity. 61
Figure 3.15– UVR of system buses after charging station connection.....61
Figure 4.1– A three-phase line.....64
Figure 4.2– The transposition of a line. 65
Figure 4.3– Partial transposition of the feeder.....68
Figure 4.4– BUVR of the system before and after partial transposition. 68
Figure 4.5– Maximum fast charging station capacity before and after partial transposition. .68
Figure 4.6– UVR of the system after and before partial transposition and after connection of charging stations. 69
Figure 4.7– BUVR of the system after and before partial transposition. 70
Figure 4.8– Maximum fast charging station capacity after and before partial transposition. .70
Figure 4.9– UVR of the system after and before partial transposition and after connection of charging stations. 70
Figure 4.10– BUVR of the system after and before partial transposition. 71
Figure 4.11– Maximum fast charging station capacity.....71
Figure 4.12– UVR of the system after partial transposition and connection of charging stations. 71
Figure 4.13– UVR of the system after modified transposition and charging station integration. 73
Figure 4.14– Comparison of fast charging station capacity between partial transposition and modified transposition. 73
Figure 4.15– UVR of the system after modified transposition.....74
Figure 4.16– Comparison of fast charging station capacity between partial transposition and modified transposition. 74

Abbreviation

BUVR	Background unbalanced voltage ratio
CC	Constant current
CC-CV	Constant current-Constant voltage
CV	Constant voltage
DG	Distribution generation
ESS	Energy storage system
EV	Electric vehicle
FCS	Fast charging station
ICE	Internal combustion engine
MSCC	Multistage constant current
PC	Pulse current
PEV	Plugged-in electric vehicle
PF	Power factor
PFC	Power factor correction
PV	Photovoltaic
PWM	Pulse width modulation
RES	Renewable energy system
THD	Total harmonic distortion
UCR	Unbalanced current ratio
UV	Unbalanced voltage
UVR	Unbalanced voltage ratio

Chapter 1

1.1 Introduction

Global warming resulting from excessive emission of industry and transportation sections has prompted to the emergence of renewable energies and plugged-in electrical vehicles (PEVs) [1]. From the transportation sector's perspective, in order to alleviate the detrimental effect of greenhouse gases, rapid substitution of eco-friendly PEVs with internal combustion engines (ICEs) is a potent solution [2]. Moreover, PEVs can greatly be effective in reducing air pollution, such that based on Energy Information Administration, their contribution can lead to the reduction of 50% to 70 % of carbon emission [3]. In spite of attracting a lot of attention for aforementioned merits, PEVs carry demerits including short range coverage, high initial cost, and long charging duration [1]. In order to overcome these obstacles and increase widespread acceptance of PEVs, many academic and industrial investigations have been conducted to fortify the infrastructures for PEVs. Some investigations are devoted to the development of the PEVs' batteries for more efficiency, longer life-span, and less loss. For example, employment of lithium-ion battery for PEVs benefits them more compared with the other batteries such as lead acid or nickel cadmium [4]. In [5], the authors have used a charging strategy to increase the efficiency of the battery. In another investigation [6], the authors claim that increasing the capacity of batteries is not a promising solution to decrease the range anxiety as the performance of PEVs will decrease due to increase in car weight. Instead, they propose a runtime power management which is contingent upon velocity, weight, and acceleration of the car. Adopting this method, the energy consumption and range anxiety would decrease [6].

In addition to improving PEVs' battery infrastructure, wide adoption of charging stations for PEVs is another alternative to tackle the mentioned problems.

The charging stations have been introduced to the market with different power levels. Generally, they are divided to two groups of slow and fast chargers. The vast integration of charging stations exposes the power system to important challenges including power unbalance, system instability, voltage deviation and power quality issues [7]. Therefore it is significantly crucial to speculate about these problems while charging stations are connected to the power system.

There are myriads of research studying the impacts of charging stations on power grid and proposing different solutions to mitigate those impacts. As for energy management and power system stability point of view, intermittent charging behaviour and load uncertainties considerably affect the power grid, thus a coordinated charging schedule is mandatory [8]. Zheng *et al.* [9] have proposed an online scheduling method to coordinate the tasks among charging station for the minimization of energy cost considering power flow and voltage constraints. There are also literatures dealing with interaction of PEVs and charging station with energy storage systems (ESSs) and renewable energy systems (RESs) to define optimization function for various objectives. In [10], the authors include the stochastic behaviour of charging stations in addition to ESSs and renewable energy systems RESs in distribution expansion planning model to minimize operational and investment cost. In order to minimize the uncertainties of charging demand, photovoltaic (PV) and ESS are installed in charging stations. In this manner, not only the integration rate of RES increases but also different planning can be made for generation and demand management [11], [12], [13]. Recently, optimal sizing and siting of charging station along with RES and ESS are attracting a lot of attentions. Islam *et al.* [14] have employed an algorithm for optimized planning of the fast charging stations. In this paper, transportation loss and power grid utility loss are minimized and optimal site and location of the fast charging stations are determined. In addition to power loss another aspect of power grid constraints such as voltage is regarded, but on the other hand the incorporation of RES and ESS are denied. A fast charging station equipped with ESS has been studied in [15]. In this paper, an optimization of ESS capacity is conducted to

minimize the station and storage cost based on the calculation of energy demand by the EV users considering their driving behaviour. Moreover, energy flow optimization between the grid and charging station has been investigated. A comprehensive allocation and sizing have been devoted to DGs, charging stations, and ESS in [16]. The authors claim that their study is the first one considering all DGs including solar and wind generation, ESS, and charging station. Another contribution of the mentioned study is consideration of time varying DGs generation and load consumption profile. Given this background, it is worth to note the other impacts of charging station on power quality and different equipment of power grid such as transformers should be taken into account. Considering harmonics, on account of employment of power electronic equipment in chargers, they are considered as nonlinear loads polluting the power system with current and voltage harmonics. [17] proposes a photovoltaic (PV) assisted fast charging station in which PV inverter is used as an active filter to reduce the harmonic of voltage and current. [18] reports harmonic contamination of current in a distribution system and claims that as the charging station capacity increases due to nonlinear characteristic of chargers, the total harmonic distortion (THD) increases as well. An algorithm for fast detection of current harmonic while PEVs are charging has been proposed by Peng *et al.* [19]. In another investigation, total harmonic distortion (THD) of current and voltage have been calculated based different modes of charging including slow, medium, and fast charging modes. The results indicate that the higher the charging level the lower the current's THD, and the THD is higher than the associated limit which is detrimental for the power grid. The proposed solution for suppression of the harmonics is employment of single-tuned filters [20]. In another study [21], a fast charger has been utilized in IEEE 34-bus benchmark and THD of voltage is calculated before and after installation of fast charging station. The results indicate that the THD rises above the permissible amount but to cope with this problem, authors have used LCL filter to mitigate the harmonics. Concerning the charging stations impacts on voltage flicker, Alshareef and Morsi [22] have conducted a research according to which charging station has been installed at the end of IEEE 4-node test feeder, and 4 different rated power of 60 kW, 150 kW, 240 kW, and 350 kW have been taken into account. The results indicate that voltage flickering violates IEEE 141 standard values at the last three rated powers. Voltage fluctuation and deviation have been investigated in [23] according to which a probabilistic arrival-time for

PEV has been taken into consideration for a charging station of 720 kW. In order to prevent voltage deviation, a capacitor bank is added to the system but this remedy does not cure voltage fluctuation. In [24], two aspects of power quality issues have been investigated. In this study the authors have adopted IEEE 34-bus benchmark for their analysis according to which the impacts of home PEVs' chargers in terms power loss and voltage deviation are studied. A coordinated charging scheme with objective of minimizing voltage deviation and power loss in residential distribution system has been employed and the results are compared with uncoordinated charging scheme. However, in this paper other aspect of power quality such as unbalance has been ignored and only the effect of slow chargers has been studied. In another study in which a field measurement has been carried out on a six bus distribution level system with four slow charging stations connected to one of the buses, and power quality measurements including harmonic, voltage flicker, and voltage/current trend are observed. The authors claim that all of the above-mentioned are stem from another buses which non-linear loads have been connected to them not from the bus with PEVs' charging station [25]. In another study [26], the effect of electric bus charging on the power distribution system a case study IEEE 33-bu is investigated. The sizing and location of the DGs are optimized using Newton-Raphson algorithm to adjust the voltage level to the standard value. Reconfiguration of feeder is an alternative method proposed in [27] to reduce the effects of the PEV charging station on overloading of the feeders, drop voltage, and power loss. Moreover, it helps with more integration of charging station for future planning. However, the effect of both charging station and reconfiguration has not been discussed in this paper. Also, in [28] methodologies are developed to analyse unbalanced phase voltage due to unbalanced line configurations and unbalanced loading level. One of the methods to mitigate unbalanced voltage in unbalanced feeders is positive/negative phase shift sequences which could be considered as partial transposition. However, this study does not consider the effect of charging stations as load in the distribution system. [29] uses the transposition of the lines in order to mitigate unbalanced voltage due to electric train. However, the conventional transposition is done, and it does not mitigate unbalanced voltage perfectly. Pinto *et al.* [30] have conducted a field power quality measurement for recharge of PEV in a residential area in Brazil. Their investigation consists of measuring power consumption, neutral current, voltage deviation and unbalance

voltage at service transformer and PEV connection point. Regarding EV connection point, the voltage deviation, THD and neutral current are not problematic concerns. Moreover, the measurement on service transformer side manifests that there is no violation in voltage magnitude, neutral current, and UVR. It is worth noting that only the effect of slow charger has been taken into account.

Given this background and with respect to ever-growing integration of PEVs and charging stations, it is highly essential to discuss power quality issues stemming from more connection of the charging stations. This is the first study investigating the effect of fast charging station on distribution system considering the behaviour of fast chargers under unbalanced input voltage. Unbalance issue can create critical problems for different equipment of power system and lead to their mal-functioning. Additionally, unbalanced current resulted from unbalanced voltage aggravates the situation and causes more damages. Thus, a comprehensive investigation is needed to overcome this problem. In the first part of the thesis, a practical fast charger of 50 kW is developed. In order to avoid high computational cost, the battery has been modelled as variable resistor that can be charged during the simulation time. Moreover, constant current-constant voltage approach has been chosen as the charging strategy. The behaviour of the charger is examined under unbalanced input voltage and is compared with normal operation of the charger. Then, the derived characteristic is utilized in power flow analysis by defining unbalanced current ratio (UCR). UCR characteristic provides the ability to model the charging station as a load in power flow analysis. In the power flow analysis the distribution system is studied based on equivalent impedance of each bus from the main source. IEEE 30-bus benchmark has been selected as the base benchmark. In order to have an exhaustive study, different feeders data from IEEE benchmarks such as IEEE 34-bus, 37-bus, and 123-bus have been utilized in the base benchmark. In order to use these data, a simplified electrical model has been proposed which uses an unbalanced impedance for simulating the feeders' data and a balanced impedance for simulating the existing loads in the system. Then, the BUVR, which is the UVR due to unbalanced feeder, for each feeder is calculated to ensure that the power system is operating under normal condition. Moreover, maximum capacity for charging station and UVR after connection of charging station are obtained while the system

is subjected to UVR and voltage constraints. The results indicate that as for IEEE 34-bus the UVR after connection of charging station reaches its maximum value of 3 % for some buses. In other words, UVR is the dominant constraint for these buses that hinders further connection of charging station to the system. However, for the other buses with lower UVR, the dominant constraint is the voltage. The simulation results for the other two cases demonstrate that all of the buses are restricted by the UVR, and the system cannot accommodate more charging station. The results imply that a promising solution is required to mitigate unbalanced voltage in the feeders for integration of charging station with higher capacity. It has been well investigated that interactions of phases of the feeders leads to mutual impedances resulting in unbalanced voltage in the feeders. Therefore, one of the promising ways to reduce the interaction is transpositions of the lines. A partial transposition has been used in this thesis according to which the feeders are divided into two equal sections. By doing the same analysis for calculation of BUVR, the results indicate that the BUVR is decreased compared to the case of non-transposed lines which results in higher capacity of charging station. However, for IEEE 37-bus and 123-bus, some buses suffer from high UVR. In other words, partial transposition is still a deficient method for these feeders.

As for another approach to mitigate the effect of mutual impedance, the involving factors for calculation of mutual impedance of the lines were investigated. In the proposed approach, the diameter and length of the feeders are optimized such that it leads to minimum mutual impedance minimizing the unbalanced voltage. This approach is called modified partial transposition. The results demonstrate that after applying modified transposition to the feeders, not only the maximum charging capacity will be increased but also UVR will be less than maximum limit. Ultimately, a power distance table is provided which enables the system operators to predict the maximum capacity for the charging station based on the distance of connection point from the main source. This table can be obtained for any system by doing the similar analysis that have been done in this thesis for different feeders' data, and provides the ability for future planning of the power system.

1.2 Thesis Overview

This thesis aims to investigate the effect of fast charging station on power systems in terms of UV. Thesis overlay has been illustrated in Figure 1.1. Chapter 2 reviews the charger topologies, and a widely used charger is employed to simulate charging characteristic of the battery. Constant current- constant voltage charging scheme is used for charging the battery and based on this algorithm, the power consumption of the charger is derived. More importantly, another objective for designing the charger is to study how the charger responses to the unbalanced input voltage then this response is used for further studies in the next chapters. Chapter 3 is dedicated to power flow analysis to obtain load flow voltage and Thevenin impedance for each bus. Then a simplified model using the data from load flow analysis is proposed such that the obtained charger's characteristic under unbalanced input voltage can be employed for unbalance studies. Based on the proposed model, in order to have a comprehensive understanding of charging stations' impacts on UV, different feeder configurations have been employed in chapter 4. It is worth noting that in all of the cases, the maximum charging station capacity is calculated such that UVR for the bus of interest would not be violated. The methodology for reducing UVR is also introduced in this chapter. In order to mitigate the adverse effect of the charging stations, a modified transposition method has been developed which not only reduces UVR but also enables the power system to adopt more charging stations and fulfil PEV owner's need. Finally, conclusions and future works are presented in chapter 5.

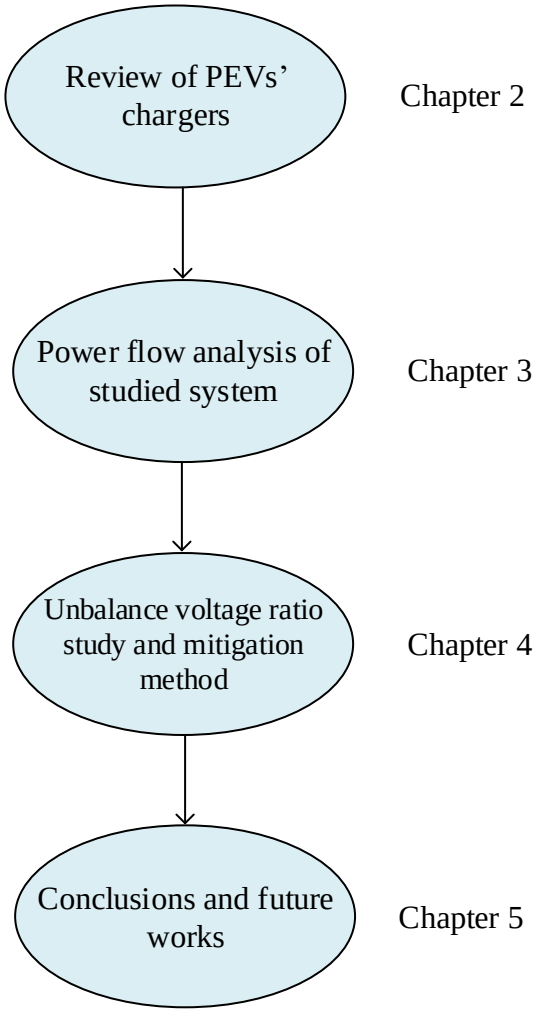

Figure 1.1– Thesis overview.

Chapter 2 Review of PEVs' Chargers

2.1 Chargers' Infrastructure

Generally, PEVs' chargers consist of AC/DC and DC/DC converters. A general schematic of the charger has been shown in Figure 2.1. As it is evident in this figure, EV chargers are divided in two groups namely, on-board (installed on the vehicle) and off-board (installed at the charging station) chargers [1]. With regard to the on-board chargers, both converter modules are mounted on the PEV, but considering the off-board chargers, the AC/DC module is installed on charging station while the DC/DC is mounted on the PEV. PEVs' charging system is also classified based on power transfer from the grid to battery, namely, conductive and inductive transfer [31]. In the former approach, cables and cords are utilized between the EVs and charging stations to transfer power. The advantages of this method are the simplicity and high efficiency. In the latter approach, there is no physical linkage between the charged object and the charging station, and the energy is transferred through induction coils based on electromagnetism principal [31]. Inductive transfer carries the merits of durability and safety.

Another method for charging the EVs is known as battery swapping. In this technique, EV owners swap their battery which may be partially charged or fully discharged with a fully charged battery. This action is done in dedicated places called battery swapping stations. This method reduces the charging process time effectively and increases battery life but, on the other hand initial investment and huge room for keeping all different batteries which should be compatible with EVs are considered as demerits of this method [32].

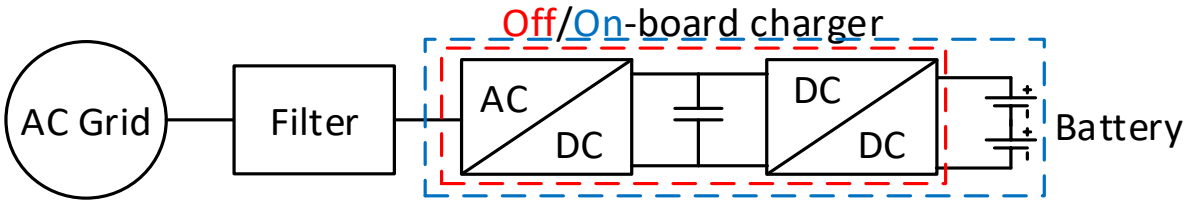

Figure 2.1– Generic schematic of a PEV charger with onboard and off board configurations.

2.2 Charging stations

Charging stations' power levels determine charging duration, location of the station, cost, needed equipment, and most importantly the effect on the power system [31]. EV charge cords, charging slots, power inlets and outlets, and connectors are considered as PEVs' supply equipment [33]. The configuration of these equipment varies from country to country which dependent on the grid codes and standards of the location [34].

2.2.1 Level 1 Charging

This charging is the slowest power one. Level 1 charging stations require single phase outlet of 120 V_{ac}, and they are installed at residential areas. The maximum power they can provide is 2 kW. They are mostly employed at overnight when there is off-peak rate in loading profile. The corresponding charging duration lays between 7-17 h [35]. The installation cost for this charging level has been estimated to be $500–$880 [36].

2.2.2 Level 2 Charging

Level 2 charging is considered as semi-fast charger which requires single or three phase outlet of 240 Vac. This type of charging station are mostly found in public areas. The maximum amount of power that they can deliver reaches 20 kW [35]. This charger is the most common charger, since its outlet supports both single and three phase connection and is installed in many public places such as hotels and shopping malls. They can provide charging time in the range

of 3-7 h to their users [35]. The installation cost for this charging level has been estimated to be $1000-$3000 [37]. Worth mentioning that level 1 and level 2 charging are on board chargers.

2.2.3 Level 3 Charging

Fast chargers cast in level 3 charging stations and they are classified by level 3 AC fast charges and level 3 DC fast chargers. The former is compatible with three phase outlet of Vac= 206-600 V and delivers maximum power of 100 kW. The latter is compatible with DC outlet of Vdc= 200-600 V and transfers maximum power of 240 kW. These chargers are installed in highways, shopping malls, and commercial places. Due to ability of providing vast amount of power, EV owners can diminish the charging time to 20 min- 1.2 h [35]. The installation cost for this charging level has been estimated to be between $30,000 and $160,000 [38]. There are different organization including society of automotive engineers (SAE) and IEEE to establish policies for transportation electrification. The above-mentioned charging levels were implemented by SAE. Table 2.1 summarizes different charger levels implemented by different standards in US and EU.

Table 2.1 – Types of charging power levels [1].

Charging Level	Charger Location	Usage	Power Level (kW)
SAE Standards			
Level 1 V_{ac}:120 V(US) V_{ac}:230 V(EU)	Single phase On-board	Residential or Office areas	P:1.9 (20 A) P:1.4 (12 A)
Level 2 V_{ac}:240 V(US) V_{ac}:400 V(EU)	Single/Three phase On-board	Public Places	P:19.2 (80 A) P:8(32 A)
Level 3 V_{ac}:206-600 V	Three phase Off-board	Commercial Area	P:50 P:100
DC fast level 1 V_{dc}:200-450 V	Off-board	Dedicated Places	P:40 (80 A)
DC fast level 2 V_{dc}:200-450 V	Off-board	Dedicated Places	P:90 (200 A)
DC fast level 3 V_{dc}:200-600 V	Off-board	Dedicated Places	P:240 (400 A)
IEC Standards			
AC Power Level 1	Single phase On-board	Residential or Office areas	P:4-7.5 (16 A)
AC Power Level 2	Single/Three phase On-board	Public Places	P:8-15 (32 A)
AC Power Level 3	Three phase On-board	Commercial Area	P:60-120 (250 A)
DC Rapid Charging	Off-board	Dedicated Places	P:100-200(400 A)

2.3 International Standards and Charging Codes for EVs

In order to reinforce the appropriate operation of chargers, promising standards and charging codes should be enacted [1]. Moreover, as standards evolve, there would be more complicated and more expensive infrastructure for chargers [39]. According to National Electrical code [35], the connectors and cables should de-energize before connecting to EVs for the first two levels of chargers. This example shows the relation between the standards and cost of hardware part of the chargers. Various organizations which have been established to prepare international standards and charging codes are as follows:

2.3.1 Society for Automotive Engineers (SAE)

- J1772: EV conductive connector and charging method.
- J2849: Issues of power quality.
- J2836/2847/2931: Communication purposes.
- J1773: Inductive coupled charging.
- J2293: Finding requirements for EV and EVSE for power delivery.

2.3.2 International Energy Agency

2.3.3 Deutsches Institut Fur Normung

- DIN 43538: Batteries' system

2.3.4 International Electrotechnical Commission (IEC)

- IEC TC 69: Regarding infrastructure of charging and safety requirements.
- IEC-1000-3-6: Issues of power quality.
- IEC TC 21: Regarding battery management.
- IEC TC 64: Electrical installation, electric shock protection.

2.3.5 Institute of Electrical and Electronic Engineers (IEEE)

- IEEE 2030.1.1: Quick DC charging for EVs.

- IEEE P2690: Charging network management, Vehicle authorization.
- IEEE P1809: Electric transportation guide.
- IEEE 1547: Interconnecting electric system with distributed resources/Tie Grid.
- IEEE 1901: Provide data rate while vehicles charged overnight.
- IEEE P2030: Interoperability of smart grid.

2.3.6 Infrastructure Working Council (IWC)

2.3.7 National Fire Protection Association (NFPA)

- NFPA 70: Safety management.
- NEC 625/626: Charging systems for EVs.
- NFPA 70E: For safety.
- NFPA 70B: Maintenance for electrical equipment.

2.4 Charger Topology

Charger components play an indispensable role in power system and charger infrastructure. Preeminent factors such as low cost, low weight, and high power factor contribute to effectiveness of charger stands. Therefore, reliable operation of the chargers is contingent upon numerous circumstances such as topologies of chargers and power electronic components, control scheme, etc [31].

Typically, chargers include several stages, namely, electromagnetic interference filter, AC/DC rectifier, power factor correction, and DC/DC converter, and each stage has its specific features. It is worth to mention that there are numerous studies dealing with topology of each stage to modify the characteristic of chargers to meet standards requirements in terms of allowable harmonic injection and power factor [31].

In terms of power direction, chargers are classified into two groups of: 1- unidirectional and 2- bidirectional chargers.

2.4.1 Unidirectional Charger

In this type of charger, active power is injected from the grid to the EV. Single and three phase diode bridges are utilized for AC/DC rectifiers to transfer the power. As that of DC/DC converter topology, series resonant converter [40], interleaved [41], etc. are utilized. The remarkable features of these chargers are simple control system, low cost, and small volume. As an example, a topology of unidirectional charger has been shown in Figure 2.2 [40].

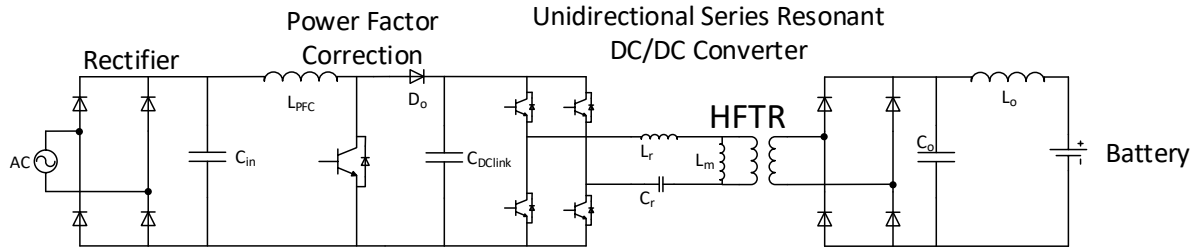

Figure 2.2– Single phase unidirectional resonant charger.

2.4.2 Bidirectional Charger

These chargers are able to transfer the power either from the grid to the EV or from EV battery to the grid. The comprising stages of the charger are the same as unidirectional charger, however, instead of utilizing diode bridges, active bridges are formed by bidirectional switches such as IGBTs. Single phase full bridge and half bridge and three phase full-bridge rectifiers are among common AC/DC rectifiers used for chargers. With regard to DC/DC converter dual active bridge, Three-level diode-clamped bidirectional are used for single phase and three phase converters [31]. As an example, a configuration of bidirectional charger has been shown in Figure 2.3.

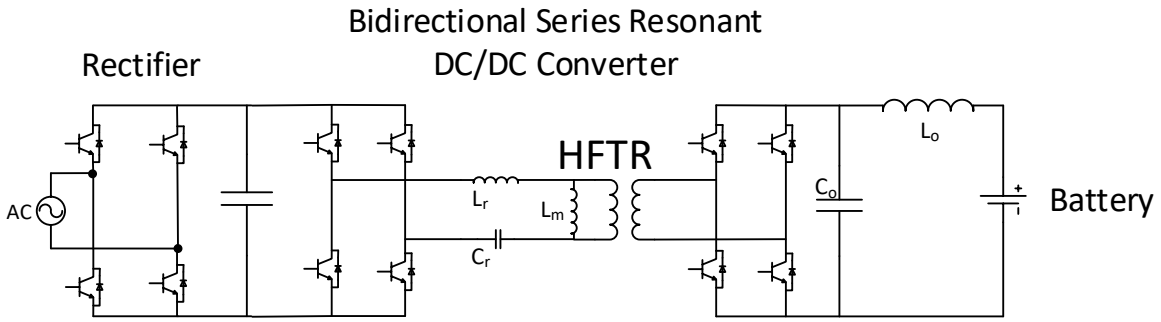

Figure 2.3– Single phase bidirectional resonant charger.

2.5 Charging Methods

Different charging methods have been developed and improved in order to decrease charging duration and the deterioration due to overcharging and increase cycle life of the batteries [42]. Charging approaches are listed below:

- Constant Current (CC)
- Constant Voltage (CV)
- Constant Current- Constant Voltage (CC-CV)
- Pulse-Current (PC)
- Multistage Constant Current (MSCC)

2.5.1 Constant Current

In this method a constant flow of current is applied to the battery, and the process is sustained till the battery voltage reaches a pre-defined value. This method may expose the battery to overheating issues because of high rate of current injection to the battery at the onset of the charging process [1].

2.5.2 Constant Voltage

In this method, a constant voltage is applied to the battery and charging current declines during charging process to a pre-set value and the process is stopped. Since the rate of current is less than CC method, overheating issues are prevented but on the other hand charging duration increases [1].

2.5.3 Constant Current- Constant Voltage

Kang *et al.* [43] combined the first two methods and created a faster and safer charging process called constant current-constant voltage. In this approach as shown in Figure 2.4 (a), the process consists of two stages; in the first stage the charging process commences by injecting a constant current to the battery till the voltage of the battery reaches a pre-set value (V_{set}).At this very moment the second stage starts. In the second stage, the pre-set voltage is fixed on battery's terminal and the current starts decaying as the battery charges. The current deteriorate till it reaches a pre-set value (around 0.1C or I_{set}) and the charging process is terminated [42].

2.5.4 Pulse Current

In this method, current pulses with a specific duty cycle are exerted to the battery, it is worth to mention that both the magnitude and duty cycle can be varied during the charging procedure [42]. The criteria for charging termination is approach of the battery voltage to a pre-determined voltage, and the frequency of pulses lays between 0.2 Hz and 100 Hz [44]. Figure 2.4 (b) shows this method of charging.

2.5.5 Multistage Constant Current

In this method, as shown in Figure 2.4 (c), the CV mode of CC-CV method is substituted by stepwise changing current. Thus, at each stage when the corresponding voltage reaches its pre-set value the current is levelled down. The charging procedures carries on till the current reduces to the pre-set value. Due to inherent feature of this method, the charging speed

decreases in compare to CC-CV but on the other hand, low cost, simplicity in control design are the advantages of this method [42].

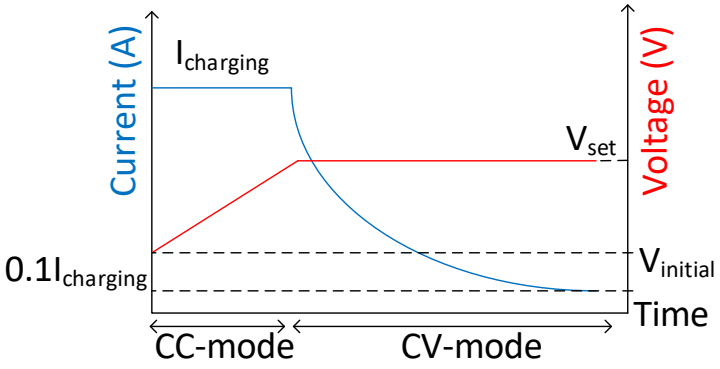

(a)

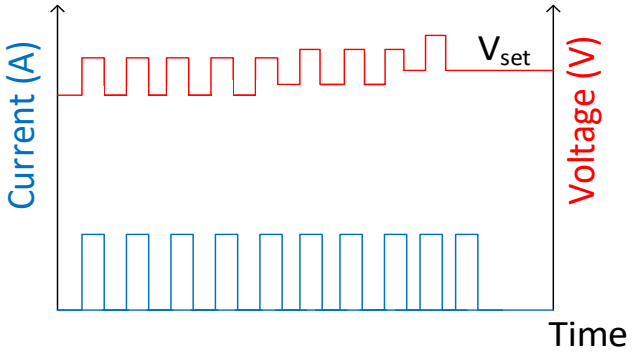

(b)

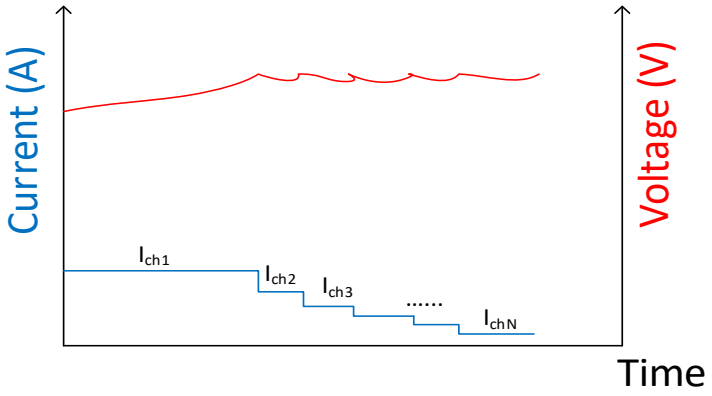

(c)

Figure 2.4– Charging methods. (a) CC-CV. (b) Pulse Current. (c) MSCC.

2.6 Charger Simulation

In this thesis, in order to observe the impacts of fast charging stations on the power system in terms of voltage drop and unbalance voltage issue, it is mandatory to investigate the behaviour of a charger i) during its operation from a type of the load perspective and ii) while an unbalanced input voltage is applied to the charger. To carry out this study, a three phase fast charger with maximum output power of 50 kW has been developed in EMTP-RV simulation environment. A three phase boost active power factor correction (PFC) AC/DC converter and a Buck DC/DC converter form the fast charger. These converters were selected since they are considered as a widely-used type of the converters. In this study, the battery is modelled as variable resistor and it is charged with CC-CV method. Figure 2.5 illustrates the simulated fast charger schematic. In the following subsection, the design of the charger and the simulation results will be discussed.

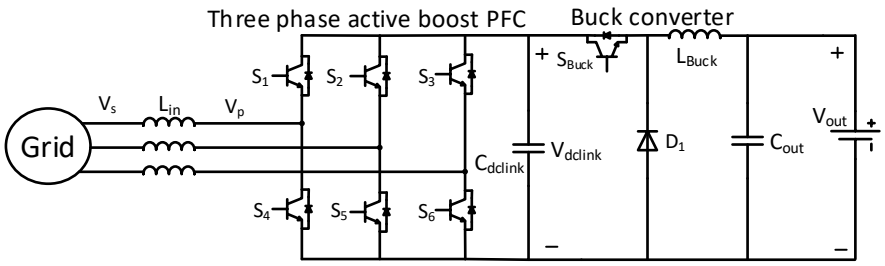

Figure 2.5– Simulated fast charger schematic.

2.6.1 AC/DC Converter Design

In this study, it is assumed that the input voltage of the charger is 480 V_{LLRMS} and the frequency of the grid is 60 Hz. With respect to the three phase active boost PFC it is preeminent to maintain the DC link voltage fixed and provide near unity PF to avoid reactive power loss in the grid. In order to achieve these two essential goals, a control system is needed. In this paper, for the sake of convenience, a simple and widely-used control system which has been developed in [21] and [45] has been utilized. The control system has been shown in Figure 2.6. In this control system, the input currents (I_a, I_b, and I_c) are transformed to *dq* frame (I_d and I_q)

using equation (2.1) in which ω is the angular frequency of the grid. Then, I_d and I_q are compared with I_{dref} and 0, respectively. It is worth to mention that I_d is responsible for maintaining output voltage at a desired value, and I_q determines the power factor. To reach this goal, PI controllers which have been shown as PI block in Figure 2.6 have been employed. Then, a *dq* to *abc* transformer is utilized (equation (2.2)) to translate PI controller outputs to sinusoidal waveforms to be compared with a sawtooth waveform and generate on-off signals for the switches. Worth mentioning that the PI coefficients are adopted from PSIM software. The parameters of the grid and the three phase active boost PFC rectifier has been shown in Table 2.2.

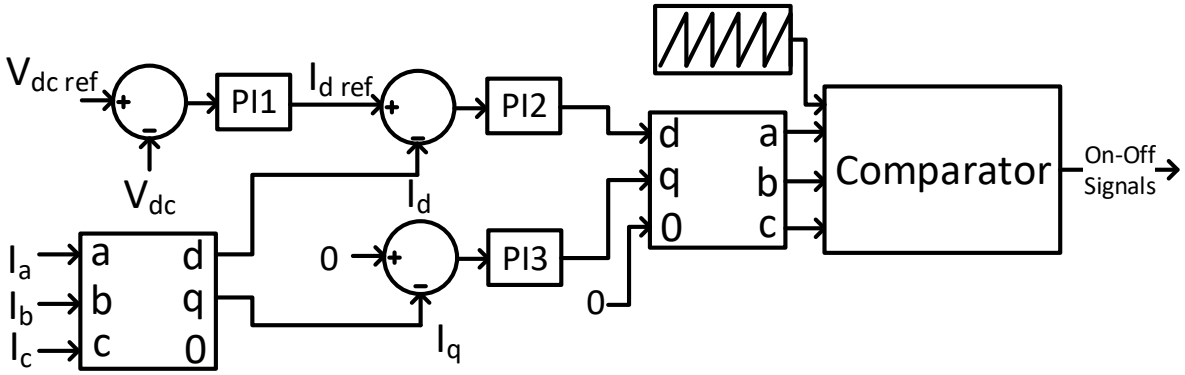

Figure 2.6– Power factor correction control system.

$$\begin{bmatrix} I_a \\ I_b \\ I_c \end{bmatrix} = \begin{bmatrix} \cos(\omega t) & -\sin(\omega t) & 1 \\ \cos(\omega t - \frac{2\pi}{3}) & -\sin(\omega t - \frac{2\pi}{3}) & 1 \\ \cos(\omega t + \frac{2\pi}{3}) & -\sin(\omega t + \frac{2\pi}{3}) & 1 \end{bmatrix} \begin{bmatrix} I_d \\ I_q \\ I_0 \end{bmatrix} \quad (2.1)$$

$$\begin{bmatrix} I_d \\ I_q \\ I_0 \end{bmatrix} = \frac{2}{3} \begin{bmatrix} \cos\theta & \cos(\theta - \frac{2\pi}{3}) & \cos(\theta + \frac{2\pi}{3}) \\ -\sin\theta & -\sin\left(\theta - \frac{2\pi}{3}\right) & -\sin\left(\theta + \frac{2\pi}{3}\right) \\ \frac{1}{2} & \frac{1}{2} & \frac{1}{2} \end{bmatrix} \begin{bmatrix} I_a \\ I_b \\ I_c \end{bmatrix} \quad (2.2)$$

Table 2.2 – Power system and AC/DC converter parameters [46], [47].

Parameter	**Value**
Grid three phase voltage	480 V_{LLRMS}
Grid frequency	60 Hz
L_{in}	1 mH
AC/DC converter switching frequency	100 kHz
DC-link voltage	800 V
DC-link capacitor	200 µF

The DC-link voltage is selected such that it should be greater than the input voltage of the converter based on equation (2.3) since otherwise the diodes of the switches will be positively biased and conduct. In the case of mal-operation, the PWM rectifier acts as a diode bridge rectifier. Thus it is necessary to keep the diode negatively biased so that they will conduct when at least one switch turns on and the instantaneous ac voltage will be favourably provided [48] and [49]. This is another major reason to employ the aforementioned controller. As that of L_{in} and C_{dclink}, the values have been selected based on literatures [46], [47] and these parameters have been modified using trial and error to provide the best answer. In equation (2.4) [50], V_{pmax} is the maximum amount of the fundamental component of the converter's ac side voltage with the characteristic of Figure 2.7, accordingly. The fundamental component is calculated by Fourier series formula (equations (2.5) and (2.6)) to obtain V_{pmax}. In equations (2.5) and (2.6), d is duty cycle. V_s is RMS phase to neutral supply voltage. $\delta_{\max}$is $\cos^{-1}(\frac{Vs}{\mathrm{Vpmax}})$, I_{dcmax}

and V_{dc} are dc current and dc voltage of the dc side of the converter, respectively. ω is the angular frequency of the grid.

$$V_{dclink} > \sqrt{2}\, V_{sLL,RMS} \tag{2.3}$$

$$L_{inmax} = \frac{3V_{pmax}V_s \sin(\delta_{\max})}{\omega V_{dclink} I_{dcmax}} \tag{2.4}$$

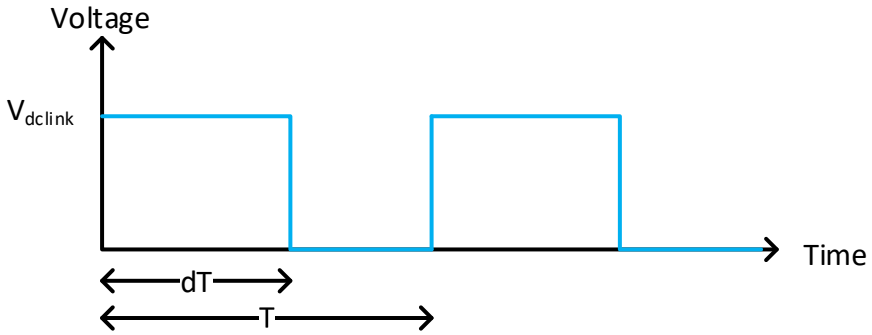

Figure 2.7– Voltage waveform of converter's switch.

$$V_{pk}|_{k=1,2,3} = V_{dclink}d + \sum_{n=1}^{\infty}\left(\frac{\sqrt{2}\, V_{dclink}}{n\pi}\sqrt{1-\cos(2\pi nd)}\sin(2\pi nft + \theta_n)\right) \tag{2.5}$$

$$\theta_n = \tan^{-1}\left(\frac{\sin(2\pi nd)}{1-\cos(2\pi nd)}\right) \tag{2.6}$$

2.6.2 DC/DC Converter Design

As shown in Figure 2.5, in this thesis a Buck converter has been employed as the DC/DC converter. This converter has a chief role in PEVs' charge since it is responsible for delivering power from the AC/DC converter to battery. In order to design the input inductor and output capacitor of the buck converter the flowing equations have been utilized [51].

$$L_{Buck} = \frac{V_{out}(V_{in} - V_{out})}{\Delta I_L \times f_s \times V_{in}} \tag{2.7}$$

$$C_{out(min)} = \frac{\Delta I_L}{8 \times f_s \times \Delta V_{out}} \tag{2.8}$$

Where, V_{in} is the input voltage of the converter, ΔI_L is inductor ripple current which is assumed to be 9 % of the maximum output current of the converter, f_s is the switching frequency, and ΔV_{out} is the desired output voltage ripple which is considered to be 10 V. Given that, the buck converter parameters are listed in Table 2.3.

Table 2.3 –DC/DC converter parameters.

Parameter	**Value**
Vin	800 V
L_{Buck}	3 mH
DC/DC converter switching frequency	5 kHz
V_{out}	350 V
C_{out}	35 μF

In this thesis, CC-CV method has been adopted for charging the simulated battery. The flowchart of this algorithm has been depicted in Figure 2.8. The battery has been modelled as

a variable resistor [52]. The charger controller has been shown in Figure 2.9 demonstrating the employed PI controllers to regulate the voltage and current.

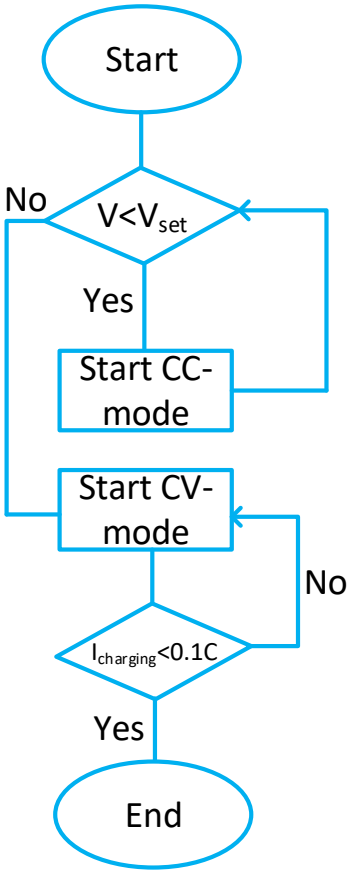

Figure 2.8– Flowchart of CC-CV charging method.

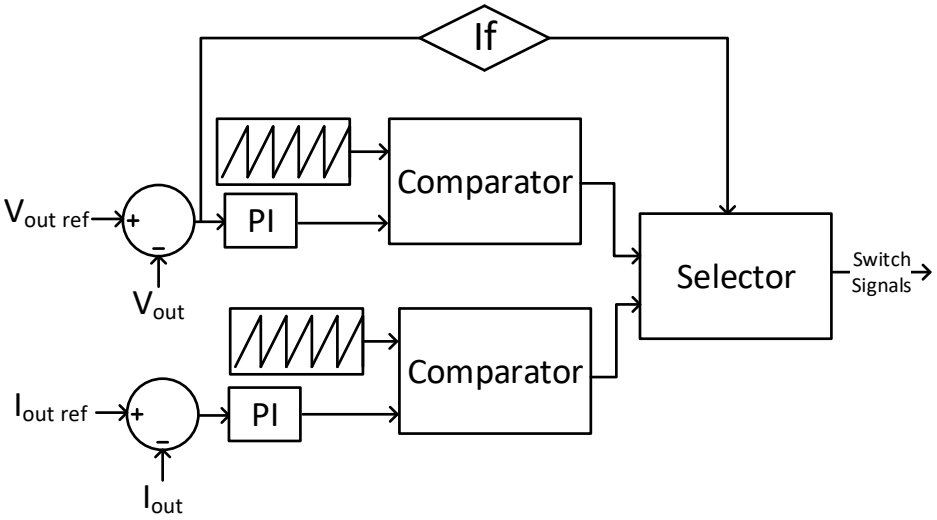

Figure 2.9– CC-CV charging controller.

2.7 Simulation results

The fast charger has been designed such that it delivers maximum power of 50 kW to the battery. As discussed in previous section, maintaining the PF close to unity and output voltage of the AC/DC converter at the desired value are the objectives of this converter. But more importantly, the main objective is to figure out the behaviour of the charger in power systems and its effects on the voltage drop and when it is fed by an unbalanced input voltage. Therefore two scenarios are conducted in this section.

2.7.1 First Scenario: Charger Operation under Normal Condition

In this scenario, the charger has been implemented in the EMTP-RV time-domain simulation environment. The duration of the simulation is 1 second and at t=0.2 s charging process commences and terminates at the very end of the simulation. During the scenario, the charger is fed by balanced input voltage, meaning that there is no negative and zero sequence in the power system. As it is evident from Figure 2.10, input current and voltage are in phase, in other words during both the CC mode and CV mode of charging process, the controller is able to provide unity power factor. Moreover, Figure 2.11 shows the THD of input current for phase

A. According to IEEE 519-2014 standard [53] the input current THD should be less than 5%. In this scenario, the input current fulfils this requirement. The other task of the AC/DC converter is to provide the desired voltage at the output of this converter. Figure 2.12 shows the dc link voltage. As it was expected, the link voltage is approximately 800 V both in CC and CV mode of charging process. It only suffers from ± 0.625 % deviation which is negligible. More importantly it does not put a significant influence on charger operation as the buck converter can operate for wide range of input voltage. The voltage and current of battery during the charging process has been shown in Figure 2.13. This figure manifests that the charging protocol is functioning properly, and one noticeable fact is that when the charging process transition from CC mode to CV mode occurs there is no violation neither in voltage nor in current of the battery.

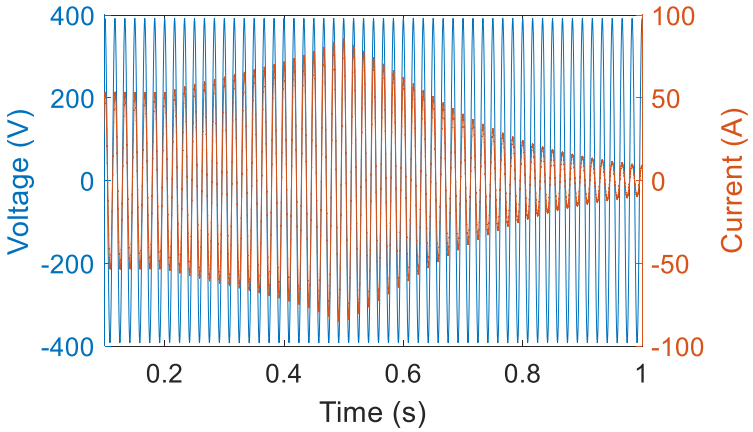

(a)

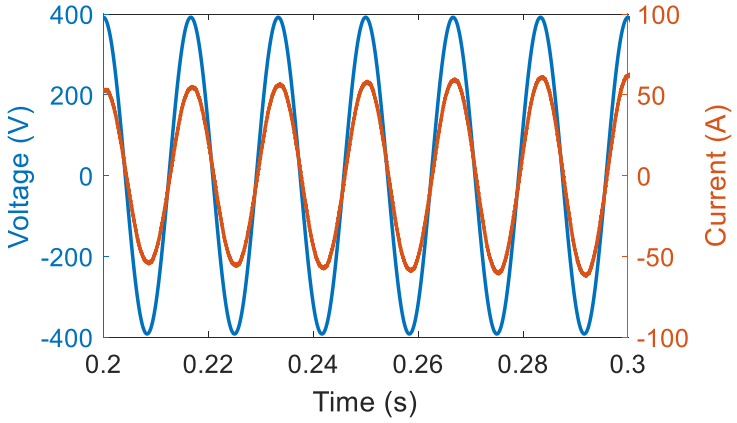

(b)

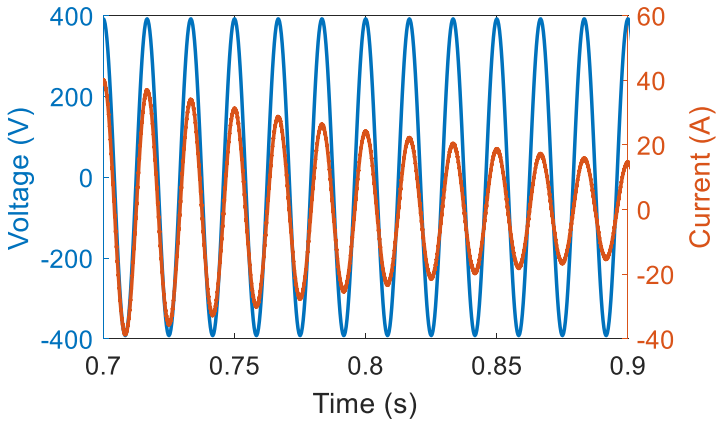

(c)

Figure 2.10– Phase input voltage and current of the charger. (a) During the whole simulation. (b) Zoomed-in during CC mode. (c) during CV mode

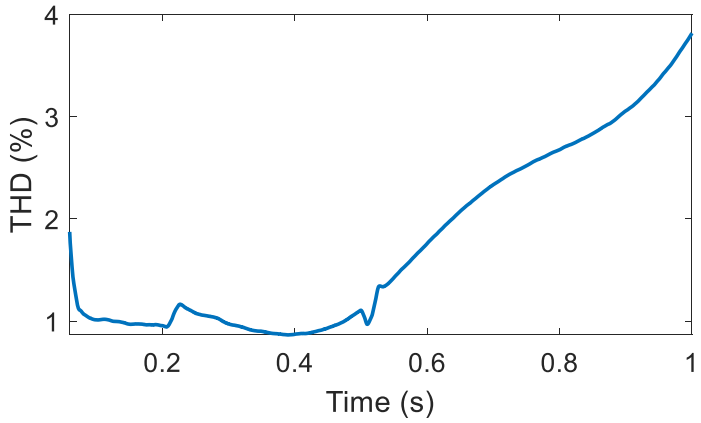

Figure 2.11– THD of input current (phase A).

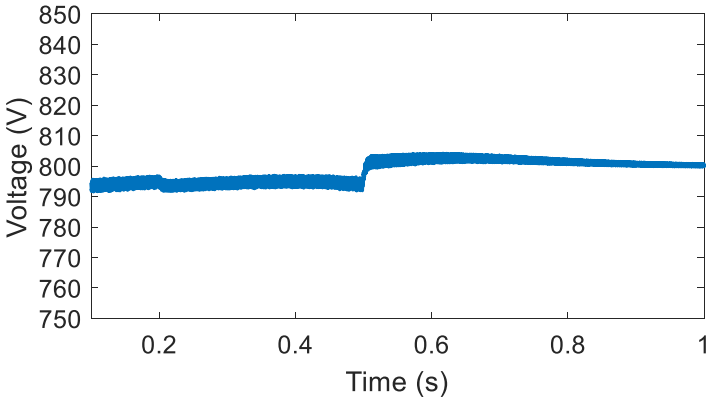

Figure 2.12– DC link voltage of AC/DC converter.

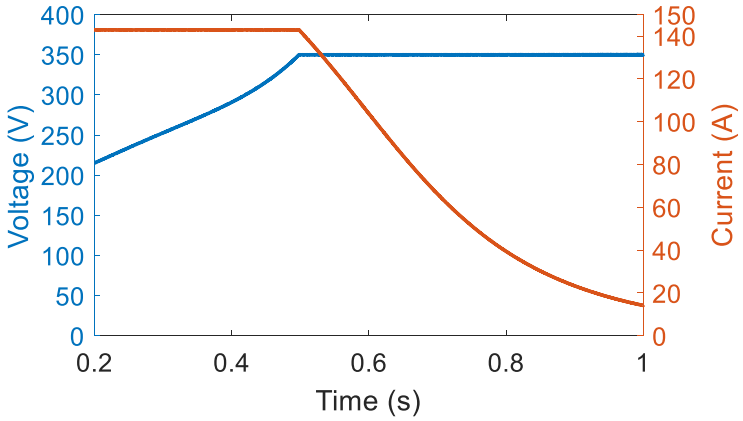

Figure 2.13– Voltage and current of battery.

2.7.2 Second Scenario: Charger Operation under Unbalanced Condition

In this scenario, the charger is fed by an unbalanced input voltage. This action is carried out by applying negative sequence voltage to the charger at t=0.25 s. More information about the relations of symmetrical sequences can be found in Appendix A [54]. This study is conducted to investigate the corresponding negative sequence current drawn from the power system by the charger. Therefore, in order to calculate the UVR the following equation has been utilized [30]:

$$UVR\% = \frac{|V_-|}{|V_+|} * 100 \tag{2.9}$$

Where $|V_-|$ and $|V_+|$ are negative and positive sequence voltage magnitudes. In this scenario it is presumed that UVR rises linearly from 0% to 10 % at the very end of the simulation. Figure 2.14 shows the UVR during the simulation.

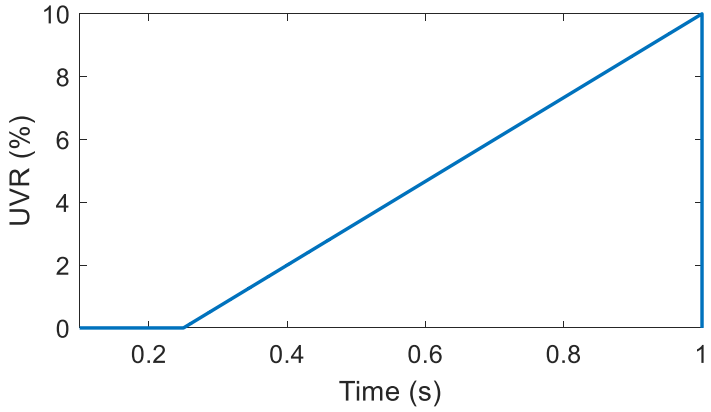

Figure 2.14– UVR percentage applied to the charger.

Figure 2.15 (a) shows the entire profile of three phase input voltage of the charger after exerting negative sequence voltage. Figure 2.15 (b) is zoom-in version of Figure 2.15 (a) at end of the simulation, since the UVR reaches its highest value. It is evident from the figure that the voltage of the phases are different from each other in term of both magnitude and phase angle.

Although the main concern of this scenario is to derive negative sequence current caused by the unbalanced input voltage, it is beneficial to investigate potential risks that UV might put on

PF, input current harmonics, and dc link voltage. Figure 2.16 demonstrates the input voltage and current for phase A. This figure starts from 0.2 s since the charging process commences at the same instant and to skip the initial transient of the charger. According to this figure, the PF will not be significantly affected by the UV. But on the other hand it seems that the current is distorted by harmonics during the CV mode. The THD of input current for phase A has been calculated and shown in Figure 2.17. One may conclude that since the URV is relatively high during the CV mode, the current suffers from the high harmonic content and does not meet the requirement for IEEE 519-2014 standard [53].

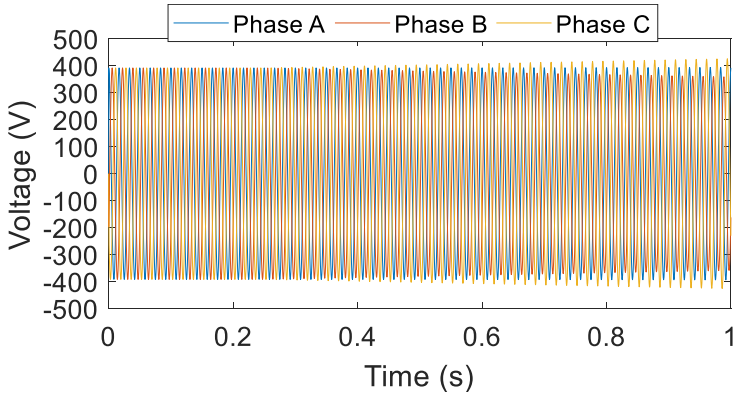

(a)

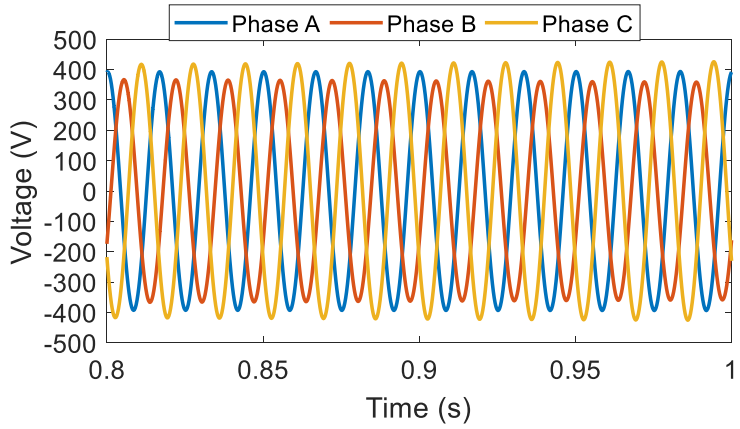

(b)

Figure 2.15– Three phase input voltage of the charger after applying negative sequence voltage.

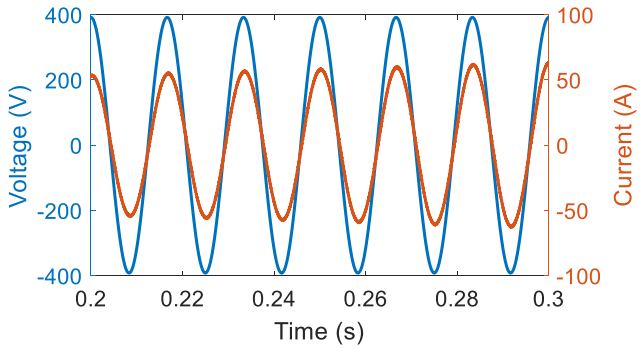

(a)

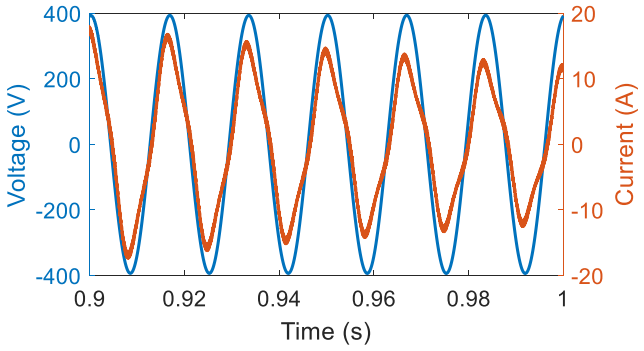

(b)

Figure 2.16– Input voltage and current of phase A after applying negative sequence voltage.

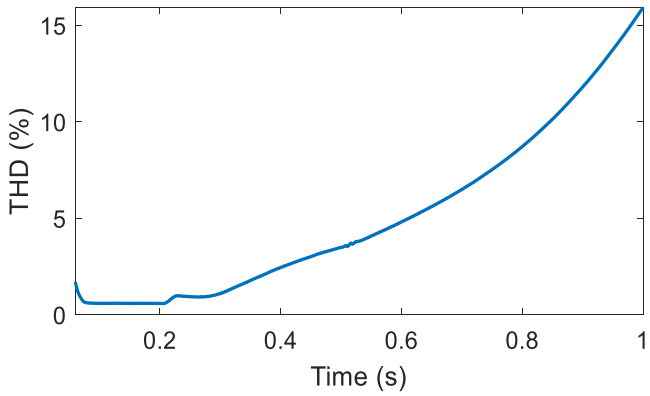

Figure 2.17– THD of input current after applying negative sequence voltage (Phase A).

The dc link voltage has been shown in Figure 2.18. Comparing this figure with Figure 2.12, it demonstrates that before imposing negative sequence voltage, the voltage of the two figure are

the same, but after applying unbalanced voltage to the charger at t=0.25 s, the dc link voltage suffers from high fluctuations.

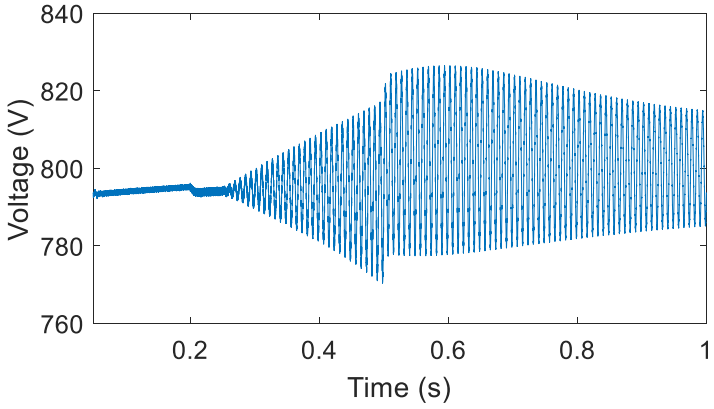

Figure 2.18– DC link voltage of AC/DC converter after applying negative sequence voltage.

Another important characteristic to be observed is the voltage and current of the battery. The aforementioned features have been plotted in Figure 2.19. As evidenced by this figure, UV does not exert any impact on current and voltage of the battery. One may deduce that in spite of high fluctuation in input voltage of the DC/DC converter, this converter operates appropriately, and the associating controllers can overcome the input voltage fluctuation and follow CC-CV charging algorithm.

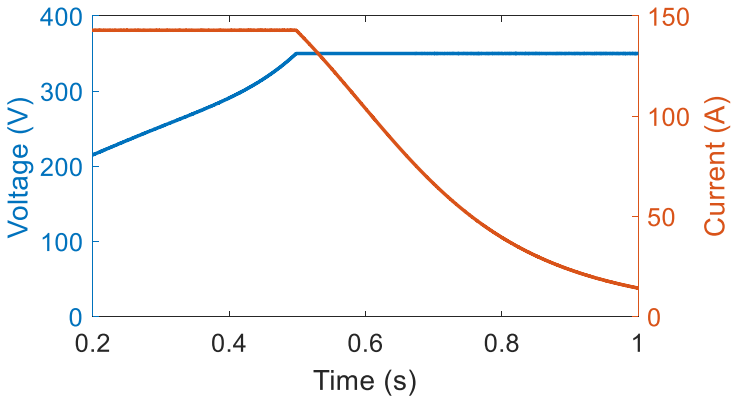

Figure 2.19– Voltage and current of the battery after applying negative sequence voltage.

In this stage, the negative sequence current stemming from unbalanced voltage is derived to be utilized in our studies in the next chapters. In order to capture this characteristic, input currents

are transformed to symmetrical sequences using the equation discussed (A.14) in A-1. Accordingly, the ratio of negative sequence current over positive sequence current, which is called unbalanced current ratio, versus time and UVR has been plotted in Figure 2.20 and Figure 2.21, respectively. It is clear from the figures that UCR increases as the UVR increases but by the end of simulation where the charger process is terminated it seems that the UCR tends to be reduced. One may conclude that despite the decreasing positive sequence current, negative sequence current remains high. This means that it is contingent upon negative sequence voltage, thus remedies should be taken into account to mitigate UVR and eventually adverse effect of UCR which will be discussed in the next chapters.

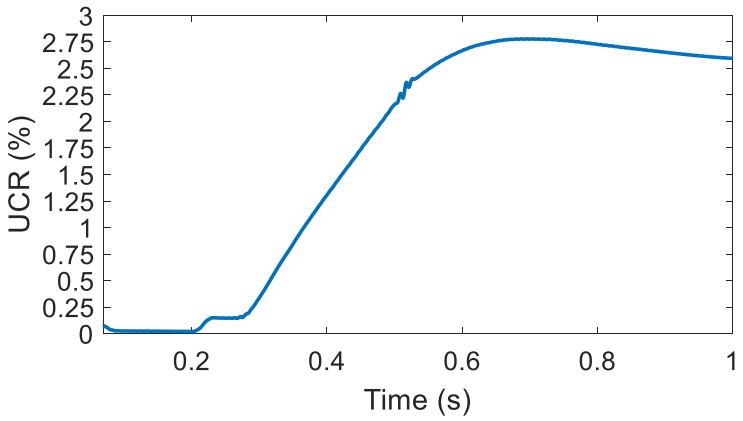

Figure 2.20– UCR of input current after applying negative sequence voltage in terms of time.

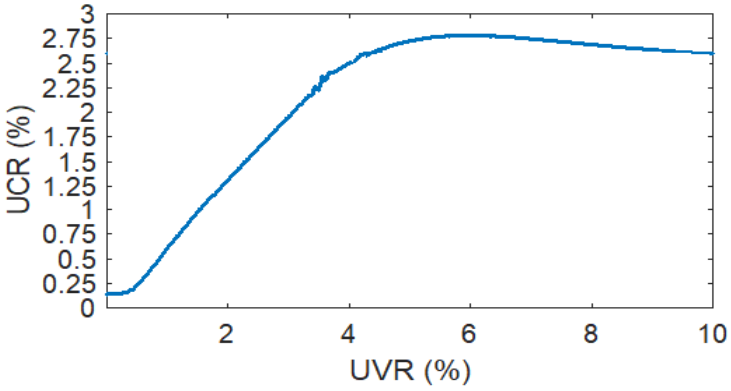

Figure 2.21– UCR of input current after applying negative sequence voltage in terms of UVR.

It is worth mentioning that in the above graph UVR and UCR have been calculated based on the rated input voltage and current, respectively.

Chapter 3 Power Flow Analysis of Studied System

3.1 Introduction

In this chapter, IEEE 30-bus system is studied under balanced conditions to obtain positive sequence voltage for each bus in the system. Then, in order to investigate the effect of fast charging station on power quality of the system, a simplified circuit is proposed. To have an all-inclusive study, different feeders from different benchmarks including IEEE 34-bus, 37-bus, and 123-bus are translated to the base benchmark (IEEE 30-bus benchmark) and the same analysis is conducted on each of them. Power flow analysis is a useful tool for future planning of the system in terms of economy, development and operation. So it is a promising way to investigate the effect of fast charging station on the system voltage drop and voltage regulation. Therefore, in this chapter power flow analysis is solved by Newton-Raphson algorithm in MATLAB.

3.2 Power Flow Solution

In order to find power system's operating conditions including line current, bus voltage, and active and reactive power, nodal solution is a promising way. Since the functions to be solved are non-linear, iterative methods are utilized to solve the equations. Therefore, in this chapter Newton-Raphson numerical method is adopted in MATLAB to analyse IEEE 30-bus power system. This method has been explicitly discussed in B.1 [54].

In power flow solution, four parameters are of interest to find. These values are voltage magnitude $|V|$, phase angle δ, active power P, and reactive power Q. Moreover the buses of the system are classified into the following types [54]:

Slack bus: There is only one slack or swing bus in the system. The voltage and phase angle of this bus is constant, and it is responsible for making equilibrium between the generated power and scheduled loads.

Load buses: Load buses are known as *PQ* buses. Active and reactive power of these buses are known while the voltage magnitude and phase angle are unknown.

Regulated buses: These buses are known as P-V bus since voltage magnitude and active power are known parameters. Reactive power and phase angle for these buses should be determined.

3.2.1 Bus Admittance Matrix

Node-voltage equations can be obtained from and expanded to a *n* bus system by following a simple example of two node circuit below:

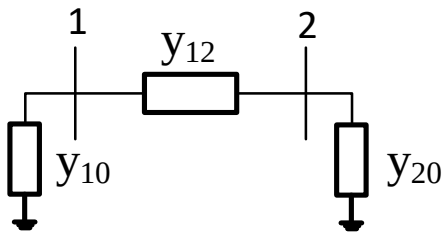

Figure 3.1– A simple circuit.

In the circuit above the admittances are in per unit on a common MVA base. Based on KCL:

$$I_1 = y_{10}V_1 + y_{12}(V_1 - V_2)$$
$$I_2 = y_{20}V_2 + y_{12}(V_2 - V_1) \quad (3.1)$$

Or

$$I_1 = (y_{10} + y_{12})V_1 - y_{12}V_2$$
$$I_2 = (y_{20}+y_{12})V_2 - y_{12}V_1 \quad (3.2)$$

Introducing the following admittance:

$$Y_{11} = y_{10} + y_{12}$$
$$Y_{22} = y_{20} + y_{12} \tag{3.3}$$
$$Y_{12} = Y_{21} = -y_{12}$$

The nodal equations reduces to

$$I_1 = Y_{11}V_1 + Y_{12}V_2$$
$$I_2 = Y_{21}V_1 + Y_{22}V_2 \tag{3.4}$$

Expanding the above equation to a n-bus system:

$$\begin{bmatrix} I_1 \\ \vdots \\ I_i \\ \vdots \\ I_n \end{bmatrix} = \begin{bmatrix} Y_{11} & \cdots & Y_{1i} & \cdots & Y_{1n} \\ \vdots & \ddots & \cdots & \cdots & \vdots \\ Y_{i1} & \cdots & \ddots & \cdots & Y_{in} \\ \vdots & \cdots & \cdots & \ddots & \vdots \\ Y_{n1} & \cdots & Y_{ni} & \cdots & Y_{nn} \end{bmatrix} \begin{bmatrix} V_1 \\ \vdots \\ V_i \\ \vdots \\ V_n \end{bmatrix} \tag{3.5}$$

Or

$$I_{bus} = Y_{bus}V_{bus} \tag{3.6}$$

Where I_{bus} is in the injected current to each bus and the sign of the current is dependent on the direction of the flow. The current is positive when it flows towards the bus and is negative when it flows away from the bus. V_{bus} is the voltage of each bus, and $Y_{bus}$is the admittance of the system where diagonal elements are called self-admittance and are equal to

$$Y_{ii} = \sum_{j=0}^{n} y_{ij} \qquad j \neq i \tag{3.7}$$

And the off-diagonal elements are known as mutual-admittance and are equal to:

$$Y_{ij} = Y_{ji} = -y_{ij} \tag{3.8}$$

The inverse of admittance matrix is called impedance matrix.

$$Z_{bus} = Y_{bus}^{-1} \tag{3.9}$$

The diagonal elements of this matrix are Thevenin equivalent impedance seen from the corresponding bus and these values are going to be employed in our study.

3.2.2 Newton-Raphson Power Flow Solution

For a typical bus of the power system which has been shown in Figure 3.2 current equation using KCL can be expressed in (3.10).

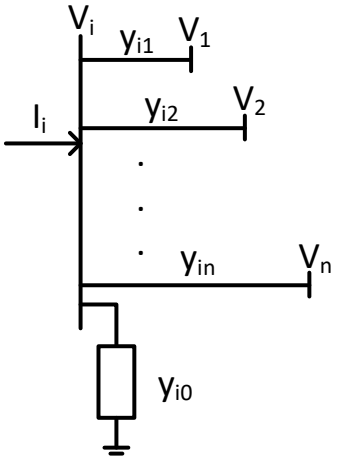

Figure 3.2– Typical bus of the power system [54].

$$I_i = y_{i0}V_i + y_{i1}(V_i - V_1) + \cdots + y_{in}(V_i - V_n)$$
$$= (y_{i0} + y_{i1} + \cdots + y_{in})V_i - y_{i1}V_1 - y_{i2}V_2 - \cdots - y_{in}V_n \quad (3.10)$$

or

$$I_i = V_i \sum_{j=0}^{n} y_{ij} - \sum_{j=1}^{n} y_{ij}V_j \qquad j \neq i \quad (3.11)$$

Active and reactive power at this bus can be calculated from:

$$P_i + jQ_i = V_i I_i^* \quad (3.12)$$

or

$$I_i = \frac{P_i - jQ_i}{V_i^*} \quad (3.13)$$

Substituting for I_i in (3.11) results in:

$$\frac{P_i - jQ_i}{V_i^*} = V_i \sum_{j=0}^{n} y_{ij} - \sum_{j=1}^{n} y_{ij} V_j \tag{3.14}$$

The above equation is non-linear equation which should be solved by Newton-Raphson algorithm.

In order to express the system electrical quantities in polar form, equation (3.10) can be written as:

$$I_i = \sum_{j=1}^{n} Y_{ij} V_j = \sum_{j=1}^{n} |Y_{ij}||V_j| \angle \theta_{ij} + \delta_j \tag{3.15}$$

The complex power at bus *i* is

$$P_i - jQ_i = I_i V_i^* \tag{3.16}$$

Substituting from (3.15) for I_i in (3.16):

$$P_i - jQ_i = (|V_i| \angle -\delta_i)) \sum_{j=1}^{n} |Y_{ij}||V_j| \angle \theta_{ij} + \delta_j \tag{3.17}$$

The real and imaginary parts of the above equation are

$$P_i = \sum_{j=1}^{n} |Y_{ij}||V_j||V_i| \cos(\theta_{ij} + \delta_j - \delta_i) \tag{3.18}$$

$$Q_i = -\sum_{j=1}^{n} |Y_{ij}||V_j||V_i| \sin(\theta_{ij} + \delta_j - \delta_i) \tag{3.19}$$

Therefor the above equation consist of independent variables. Two equations ((3.18) and (3.19)) are used for PQ buses and equation (3.18) is used for P-V buses. If we expand the above mentioned equations by Taylor's series around the initial estimate and neglect high-order terms, the following matrix result:

$$\begin{bmatrix} \Delta P_2^{(k)} \\ \vdots \\ \Delta P_n^{(k)} \\ \hline \Delta Q_2^{(k)} \\ \vdots \\ \Delta Q_n^{(k)} \end{bmatrix} = \left[\begin{array}{ccc|ccc} \frac{\partial P_2^{(k)}}{\partial \delta_2} & & \frac{\partial P_2^{(k)}}{\partial \delta_n} & \frac{\partial P_2^{(k)}}{\partial |V_2|} & & \frac{\partial P_2^{(k)}}{\partial |V_n|} \\ \vdots & & \vdots & \vdots & & \vdots \\ \frac{\partial P_n^{(k)}}{\partial \delta_2} & \cdots & \frac{\partial P_n^{(k)}}{\partial \delta_n} & \frac{\partial P_n^{(k)}}{\partial |V_2|} & \cdots & \frac{\partial P_n^{(k)}}{\partial |V_n|} \\ \hline \frac{\partial Q_2^{(k)}}{\partial \delta_2} & & \frac{\partial Q_2^{(k)}}{\partial \delta_n} & \frac{\partial Q_2^{(k)}}{\partial |V_2|} & & \frac{\partial Q_2^{(k)}}{\partial |V_n|} \\ \vdots & & \vdots & \vdots & & \vdots \\ \frac{\partial Q_n^{(k)}}{\partial \delta_2} & & \frac{\partial Q_2^{(k)}}{\partial \delta_n} & \frac{\partial Q_n^{(k)}}{\partial |V_2|} & & \frac{\partial Q_n^{(k)}}{\partial |V_n|} \end{array}\right] \begin{bmatrix} \Delta \delta_2^{(k)} \\ \vdots \\ \Delta \delta_n^{(k)} \\ \hline \Delta \left|V_2^{(k)}\right| \\ \vdots \\ \Delta \left|V_n^{(k)}\right| \end{bmatrix} \tag{3.20}$$

Slack bus is considered as bus number 1 and since the voltage magnitude and phase angle for this bus is known, the above equation does not contain bus1. In the short form we have the following equation:

$$\begin{bmatrix} \Delta P \\ \Delta Q \end{bmatrix} = \begin{bmatrix} J_1 & J2 \\ J3 & J4 \end{bmatrix} \begin{bmatrix} \Delta \delta \\ \Delta |V| \end{bmatrix} \tag{3.21}$$

After solving the above matrix, new phase angle and voltage magnitude are calculated by following equations:

$$\delta_i^{(k+1)} = \delta_i^{(k)} + \Delta \delta_i^{(k)} \tag{3.22}$$

$$\left|V_i^{(k+1)}\right| = \left|V_i^{(k)}\right| + \Delta \left|V_i^{(k)}\right| \tag{3.23}$$

The procedure goes on until the convergence criteria are met:

$$\left|\Delta P_i^{(k)}\right| \leq \epsilon \tag{3.24}$$

$$\left|\Delta Q_i^{(k)}\right| \leq \epsilon \tag{3.25}$$

3.2.3 Studied System Data

In this thesis, IEEE 30-bus benchmark is of interest. It is essential for our study to investigate system conditions in terms of voltage stability and UV before integration of any fast charging station to the system. Figure 3.3 shows the single line diagram of IEEE 30-bus system in which the placement of the loads and generators have been indicated.

The system data for initial estimate of voltage magnitude and phase angle of the buses and type of the buses, and line parameters have been listed in Table 3.1 and

9	3	1	0	0	0	0	0	0	0
10	3	1	0	0	19	5.8	2	0	0
11	2	1.082	0	0	16.2	0	0	-6	24
12	3	1	0	0	0	11.2	7.5	0	0
13	2	1.071	0	0	10.6	0	0	-6	24
14	3	1	0	0	0	6.2	1.6	0	0
15	3	1	0	0	0	8.2	2.5	0	0
16	3	1	0	0	0	3.5	1.8	0	0
17	3	1	0	0	0	9	5.8	0	0
18	3	1	0	0	0	3.2	0.9	0	0
19	3	1	0	0	0	9.5	3.4	0	0
20	3	1	0	0	0	2.2	0.7	0	0
21	3	1	0	0	0	17.5	11.2	0	0
22	3	1	0	0	0	0	0	0	0
23	3	1	0	0	0	3.2	1.6	0	0
24	3	1	0	0	4.3	8.7	6.7	0	0
25	3	1	0	0	0	0	0	0	0
26	3	1	0	0	0	3.5	2.3	0	0
27	3	1	0	0	0	0	0	0	0

28	3	1	0	0	0	0	0	0	0
29	3	1	0	0	0	2.4	0.9	0	0
30	3	1	0	0	0	10.6	1.9	0	0

Table 3.2, respectively.

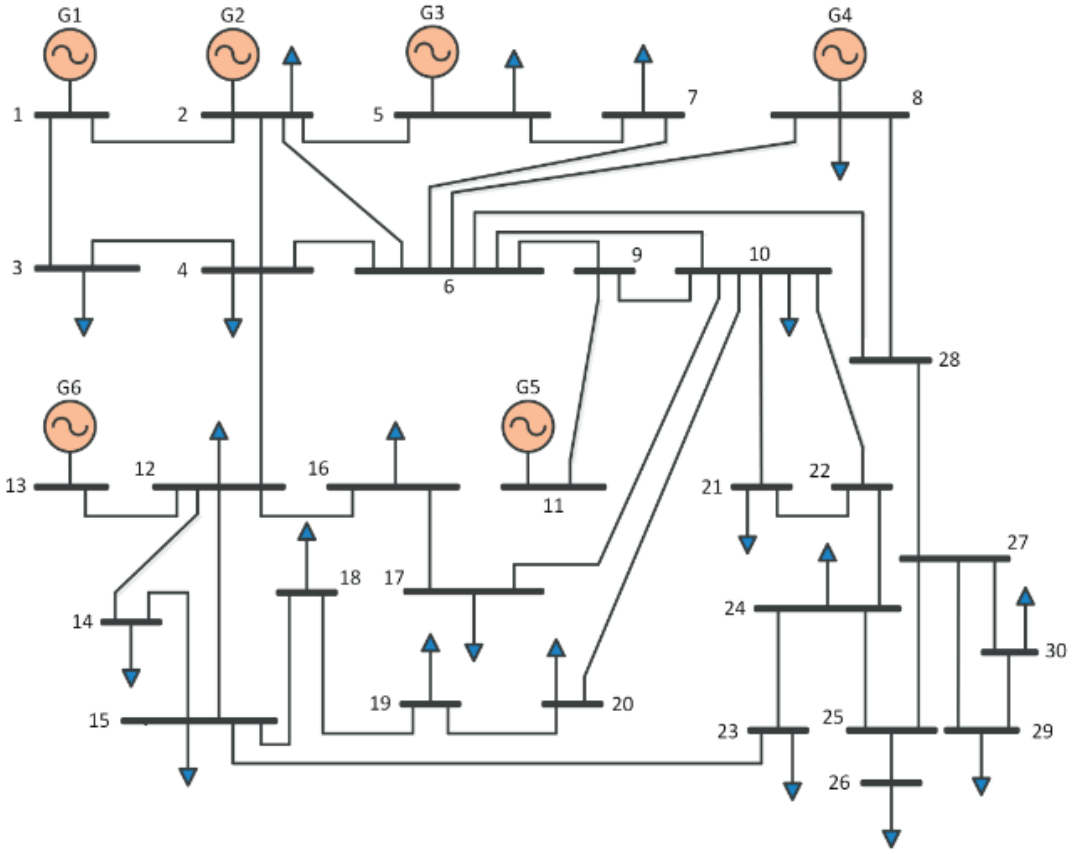

Figure 3.3– One line diagram of IEEE 30-bus benchmark [55].

Table 3.1 –Bus data for IEEE 30-bus benchmark.

Bus	**Type**	**V**	**Theta**	**P_{Gi}**	**Q_{Gi}**	**P_{Li}**	**Q_{Li}**	**Q_{min}**	**Q_{max}**
1	1	1.06	0	0	0	0	0	0	0
2	2	1.043	0	40	50	21.7	12.7	-40	50
3	3	1	0	0	0	12.4	1.2	0	0
4	3	1.06	0	0	0	7.6	1.6	0	0
5	2	1.01	0	0	37.3	94.2	19	-40	40

6	3	1	0	0	0	0	0	0	0
7	3	1	0	0	0	22.8	10.9	0	0
8	2	1.01	0	0	37.3	30	30	-10	40
9	3	1	0	0	0	0	0	0	0
10	3	1	0	0	19	5.8	2	0	0
11	2	1.082	0	0	16.2	0	0	-6	24
12	3	1	0	0	0	11.2	7.5	0	0
13	2	1.071	0	0	10.6	0	0	-6	24
14	3	1	0	0	0	6.2	1.6	0	0
15	3	1	0	0	0	8.2	2.5	0	0
16	3	1	0	0	0	3.5	1.8	0	0
17	3	1	0	0	0	9	5.8	0	0
18	3	1	0	0	0	3.2	0.9	0	0
19	3	1	0	0	0	9.5	3.4	0	0
20	3	1	0	0	0	2.2	0.7	0	0
21	3	1	0	0	0	17.5	11.2	0	0
22	3	1	0	0	0	0	0	0	0
23	3	1	0	0	0	3.2	1.6	0	0
24	3	1	0	0	4.3	8.7	6.7	0	0
25	3	1	0	0	0	0	0	0	0
26	3	1	0	0	0	3.5	2.3	0	0
27	3	1	0	0	0	0	0	0	0
28	3	1	0	0	0	0	0	0	0
29	3	1	0	0	0	2.4	0.9	0	0
30	3	1	0	0	0	10.6	1.9	0	0

Table 3.2 – Line data for IEEE 30-bus benchmark.

From Bus	**To Bus**	**R (pu)**	**X (pu)**	**B/2 (pu)**	**Tap changer (a)**
1	2	0.0192	0.0575	0.0264	1
1	3	0.0452	0.1652	0.0204	1
2	4	0.057	0.1773	0.0184	1
3	4	0.0132	0.0379	0.0042	1

2	5	0.0472	0.1983	0.0209	1
2	6	0.0581	0.1763	0.0187	1
4	6	0.0119	0.0414	0.0045	1
5	7	0.046	0.116	0.0102	1
6	7	0.0267	0.082	0.0085	1
6	8	0.012	0.042	0.0045	1
6	9	0	0.208	0	0.978
6	10	0	0.556	0	0.969
9	11	0	0.208	0	1
9	10	0	0.11	0	1
4	12	0	0.256	0	0.932
12	13	0	0.14	0	1
12	14	0.1231	0.2559	0	1
12	15	0.0662	0.304	0	1
12	16	0.0945	0.1987	0	1
14	15	0.221	0.1997	0	1
16	17	0.824	0.1923	0	1
15	18	0.1073	0.2185	0	1
18	19	0.0639	0.1292	0	1
19	20	0.034	0.068	0	1
10	20	0.0936	0.209	0	1
10	17	0.0324	0.0845	0	1
10	21	0.0348	0.0749	0	1
10	22	0.0727	0.1499	0	1
21	23	0.0116	0.0236	0	1
15	23	0.1	0.202	0	1
22	24	0.115	0.179	0	1
23	24	0.132	0.27	0	1
24	25	0.1885	0.3292	0	1
25	26	0.2544	0.38	0	1
25	27	0.1093	0.2087	0	1
28	27	0	0.396	0	0.968

27	29	0.2198	0.4153	0	1
27	30	0.3202	0.6027	0	1
29	30	0.2399	0	0	1
8	28	0.0636	0.2	0.0214	1
6	28	0.0169	0.0599	0.065	1

In Table 3.1, type 1 is the slack bus, type 2 and type3 are P-V and PQ bus types, respectively. P_{Gi} and Q_{Gi} are the generated active and reactive powers at bus *i*, respectively. P_{Li} and Q_{Li} are scheduled active and reactive powers of the load at bus *i*, respectively. Eventually, Q_{min} and Q_{max} are minimum and maximum reactive powers for P-V buses to generate or consume. In Table 3.2, R, X, and B are resistance, inductance, and susceptance of the each section, respectively. Tap changer ratios are utilized to compensate voltage drop in the lines from one bus to another.

Given this background, voltage magnitude and phase angle of all buses are obtained by power flow analysis and are listed in Table 3.3. These two values are taken into account since this study aims to investigate the effect of fast charging station on the voltage drop and UV of the system. Thus, it is preeminent to be assured that the power system operates without any violation, under normal conditions. In this thesis, it is assumed that the bus voltages are subjected to the following constraint:

$$V_{i,min} \leq V_i \leq V_{i,max} \tag{3.26}$$

where $V_{i,min}$ and $V_{i,max}$ are acceptable minimum and maximum voltage for each bus, and are considered to be 0.94 pu and 1.06 pu , respectively. Another constraints to be taken into consideration is the bus UVR which should be less than 3%, according to [30].

$$UVR_i \leq 3\% \quad i = i_{th}\ bus \tag{3.27}$$

Table 3.3 –Voltage magnitude and phase angle of buses.

Bus number	Voltage magnitude (PU)	Phase angle (Radian)
1	1.06000000000000	0
2	1.04300000000000	-0.093329865290079

3	1.02167525354617	-0.131682084574441
4	1.01292003367193	-0.162297253909451
5	1.01000000000000	-0.247037498288121
6	1.01208404921763	-0.193522455818889
7	1.00346757096807	-0.224682474120420
8	1.01000000000000	-0.206016653734980
9	1.05072386265965	-0.246725783384267
10	1.04375822323106	-0.274612497716169
11	1.08200000000000	-0.246725783384267
12	1.05760459333750	-0.260780212488752
13	1.07100000000000	-0.260780212488752
14	1.04287919933158	-0.276187549236744
15	1.03844462257161	-0.277683300436243
16	1.04451977839670	-0.271376277837106
17	1.03865357452134	-0.277256711489410
18	1.02815793085378	-0.288720252363474
19	1.02521032012796	-0.291946384717171
20	1.02906226753052	-0.288612486495189
21	1.02926054918307	-0.283550412420992
22	1.03528849545803	-0.280540190800211
23	1.02913413639521	-0.283665572535845
24	1.02365162730254	-0.286947064013502
25	1.02015660273942	-0.280193761023655
26	1.00253007325140	-0.287477022457034
27	1.02651795677777	-0.271499328026698
28	1.01086397688358	-0.204965097147239
29	1.00674903362462	-0.292826604855710
30	0.995314695636118	-0.308131659437778

The results in Table 3.3 demonstrate that the voltage of the buses are within the acceptable range except for some P-V buses which their voltages are fixed at predetermined values.

It is also worth mentioning that since line sections connecting the buses of the system are balanced and there is no unbalanced load in the system, the UVR for all of the buses is equal to zero which is less than 3 %.

3.2.4 Investigation of System Behaviour with Unbalanced Feeders

Typically in reality the feeders are not balanced and in addition to zero, positive, and negative sequence impedances, they have mutual impedance resulting from mutual interaction of phase's lines. Thus, the impedance matrix will be:

$$Z_{feeder} = \begin{bmatrix} Z_{00} & Z_{01} & Z_{02} \\ Z_{10} & Z_{11} & Z_{12} \\ Z_{20} & Z_{21} & Z_{22} \end{bmatrix} \tag{3.28}$$

Using Z_{feeder} in the following equation:

$$\begin{bmatrix} V_0 \\ V_1 \\ V_2 \end{bmatrix} = \begin{bmatrix} Z_{00} & Z_{01} & Z_{02} \\ Z_{10} & Z_{11} & Z_{12} \\ Z_{20} & Z_{21} & Z_{22} \end{bmatrix} \begin{bmatrix} I_0 \\ I_1 \\ I_2 \end{bmatrix} \tag{3.29}$$

This matrix implies that due to mutual interaction of the feeder's lines and negative sequence impedance, the consequence will be rising of the negative sequence voltage and accordingly increasing in UVR of the system.

In order to have a comprehensive investigation of the effect of unbalanced feeders on the studied system, different feeders' information of the other benchmarks are utilized such that the Thevenin positive sequence impedance of the base system (IEEE 30-bus benchmark) should remain the same at each feeder's impedance matrix and other elements of the matrix should be accordingly scaled. This action is carried out to best simulate the studied system with the unbalanced feeders.

In order to employ the other benchmarks' feeders and obtain the corresponding negative sequence voltage, a simplified model has been proposed and shown in Figure 3.4.

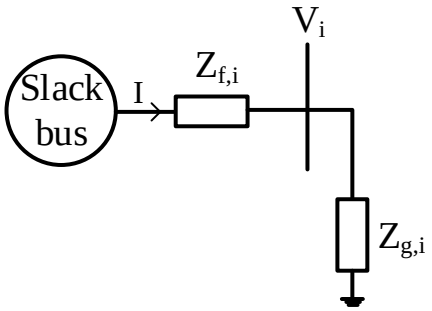

Figure 3.4– Simplified proposed model.

This model has been implemented to simulate feeder impedance for each bus individually and investigate the effect of unbalanced feeder on UVR of the corresponding bus. In Figure 3.4, the equivalent impedance seen from bus *i* is:

$$Z_{Thevenin,i} = Z_{f,i} || Z_{g,i} \tag{3.30}$$

Where $Z_{Thevenin,i}$ is equal to diagonal elements of Z_{bus} matrix. Moreover, V_i is the voltage of i_{th} bus from Table 3.3 and V_{slack}=1.06. The voltage division between $Z_{f,i}$ and $Z_{g,i}$ yields to

$$\frac{Z_{g,i}}{Z_{g,i} + Z_{f,i}} = \frac{V_i}{V_{slack}} \tag{3.31}$$

Solving equations (3.30) and (3.31), the values of $Z_{f,i}$ and $Z_{g,i}$ for each bus are obtained. $Z_{f,i}$ is utilized for translating other feeders data to the existing one, and $Z_{g,i}$ is considered as a balanced and symmetric load, so this matrix only contains diagonal elements which are equal to each other .

$$Z_{f,i} = \begin{bmatrix} Z_{f00,i} & Z_{f01,i} & Z_{f02,i} \\ Z_{f10,i} & Z_{f11,i} & Z_{f12,i} \\ Z_{f20,i} & Z_{f21,i} & Z_{f22,i} \end{bmatrix} \tag{3.32}$$

$$Z_{g,i} = \begin{bmatrix} Z_{g00,i} & 0 & 0 \\ 0 & Z_{g11,i} & 0 \\ 0 & 0 & Z_{g22,i} \end{bmatrix} \tag{3.33}$$

This allows to evaluate the system along with integration of fast charging station in terms of voltage drop and UV. In order to obtain positive and negative sequence voltage of the proposed

model, KVL equation are used to extract the aforementioned voltages. It is worth to mention that the zero sequence voltage is not considered in this study as the system is grounded and there is no zero sequence current flowing in the system. Additionally Z_{01} and Z_{02} in (3.29) are relatively small and do not contribute to create a significant zero sequence voltage. Thus, KVL equation for positive and negative sequence of the proposed model for i_{th} bus is:

$$\begin{bmatrix}1.06\\0\end{bmatrix}=\begin{bmatrix}Z_{f11,i} & Z_{f12,i}\\ Z_{f21,i} & Z_{f22,i}\end{bmatrix}\begin{bmatrix}I_{1,i}\\I_{2,i}\end{bmatrix}+\begin{bmatrix}V_{1,i}\\V_{2,i}\end{bmatrix} \tag{3.34}$$

Where $I_{1,i}$ and $I_{2,i}$ are positive and negative sequence of current I shown in Figure 3.4, respectively. $V_{1,i}$ and $V_{2,i}$ are positive sequence of voltage V_i, respectively. $I_{1,i}$ and $I_{2,i}$ can be calculated by:

$$\begin{aligned} I_{1,i}&=\frac{V_{1,i}}{Z_{g11,i}}\\ I_{2,i}&=\frac{V_{2,i}}{Z_{g11,i}}\end{aligned} \tag{3.35}$$

Substituting for $I_{1,i}$ and $I_{2,i}$ in (3.34) results in:

$$\begin{bmatrix}1.06-V_{1,i}\\0-V_{2,i}\end{bmatrix}=\begin{bmatrix}Z_{f11,i} & Z_{f12,i}\\ Z_{f21,i} & Z_{f22,i}\end{bmatrix}\begin{bmatrix}\frac{V_{1,i}}{Z_{g11,i}}\\ \frac{V_{2,i}}{Z_{g11,i}}\end{bmatrix} \tag{3.36}$$

Or

$$\begin{aligned} 1.06-V_{1,i}-Z_{f11,i}\frac{V_{1,i}}{Z_{g11,i}}-Z_{f12,i}\frac{V_{2,i}}{Z_{g11,i}}&=0\\ V_{2,i}+Z_{f21,i}\frac{V_{1,i}}{Z_{g11,i}}+Z_{f22,i}\frac{V_{2,i}}{Z_{g11,i}}&=0\end{aligned} \tag{3.37}$$

In order to obtain the negative and positive sequence voltage at each bus the above equations should be solved. In this study these equations are solve by Newton-Raphson method, and UVR is obtained.

In the following subsections IEEE 34-bus, 37-bus, 123-bus feeders are translated to 30-bus system and voltage drop and UVR are investigated for different feeders. In this case, the integration of fast charging station to the system is avoided so that the BUVR can be calculated. In other words, BUVR is the unbalanced voltage ratio stemming from the unbalanced feeders without connection of any additional load to the system. It is worthy to clarify that since V_i (in Figure 3.4) is calculated by power flow analysis, it means that the existing loads of the system are included, thus the change of the feeders does not change positive sequence voltage, however it causes the increase of negative sequence voltage which may exceed the acceptable limit. Thus it is required to first investigate BUVR for the aforementioned feeders and then find the maximum capacity of the fast charging station that can be connected to the system without threatening power quality and voltage stability which means that the system should be subjected to the constraints (3.26) and (3.27).

3.2.4.1 General Information for Feeders

3.2.4.1.1 Overhead spacing model

Different kinds of overhead lines are listed in Table 3.4 [56]. Accordingly, the schematic of spacing IDs listed in Table 3.4 have been shown in Figure 3.5. In this figure, the distance between the phase conductors and the neutral conductor have been shown in inches.

Table 3.4 – Overhead line spacing.

Spacing ID	Type
500	Three-Phase, 4 wire
505	Two-Phase, 3 wire
510	Single-Phase, 2 wire

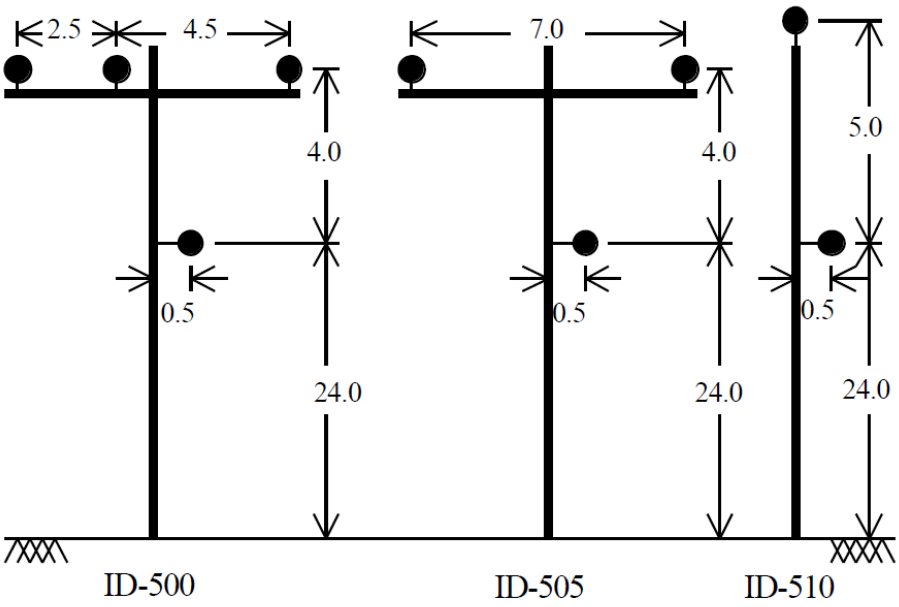

Figure 3.5– Overhead line spacing [56].

3.2.4.1.2 Conductor Data

Various conductors' characteristic have been listed in Table 3.5. The columns data correspond to [56]:

1 – Conductor size in AWG or kcmil

2 – Type of conductor

AA = All Aluminum

ACSR = Aluminum Conductor Steel Reinforced

CU = Copper

3 – 60 Hz resistance at 50 degrees C (ohms/mile)

4 – Conductor outside diameter (inches)

5 – Geometric Mean Radius (ft.)

6 – Ampacity at 50 degrees C (amps)

Table 3.5 – Conductor Data.

1	2	3	4	5	6
1000	AA	0.105	1.15	0.0368	698
556.5	ACSR	0.1859	0.927	0.0313	730
500	AA	0.206	0.813	0.026	483
336.4	ACSR	0.306	0.721	0.0244	530
250	AA	0.410	0.567	0.0171	329
# 4/0	ACSR	0.592	0.563	0.00814	340
# 2/0	AA	0.769	0.414	0.0125	230
# 1/0	ACSR	1.12	0.398	0.00446	230
# 1/0	AA	0.97	0.368	0.0111	310
# 2	AA	1.54	0.292	0.00883	156
# 2	ACSR	1.69	0.316	0.00418	180
# 4	ACSR	2.55	0.257	0.00452	140
# 10	CU	5.903	0.102	0.00331	80
# 12	CU	9.375	0.081	0.00262	75
# 14	CU	14.872	0.064	0.00208	20

3.2.4.1.3 Cable Spacing Models:

Cable different types and the spacing ID numbers are listed in Table 3.6 [56]. Figure 3.6 shows the corresponding spacing IDs.

Table 3.6 –Cable spacing.

Spacing ID	Type
515	Three-Phase, 3 cable
520	Two-Phase, 2 cable

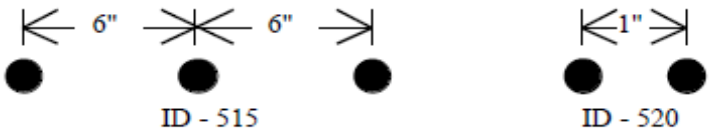

Figure 3.6–Cable spacing [56].

3.2.4.1.4 Cable Data

The features of different neutral cables are listed in Table 3.7, and the column numbers are matched with the following descriptions:

1 – Conductor size in AWG or kcmil

2 – Diameter over insulation (inches)

3 – Diameter over screen (inches)

4 – Outside diameter (inches)

5 – Copper 1/3 neutral (No. x AWG)

6 – Ampacity in 4 inch duct

Table 3.7 – Neutral 15 kV All Aluminum (AA) Cable.

1	2	3	4	5	6
2(7x)	0.78	0.85	0.98	6 x 14	135
1/0(19x)	0.85	0.93	1.06	6 x 14	175
2/0(19x)	0.90	0.97	1.10	7 x 14	200
250(37x)	1.06	1.16	1.29	13 x 14	260
500(37x)	1.29	1.39	1.56	16 x 12	385
1000(61x)	1.64	1.77	1.98	20 x 10	550

3.2.4.2 IEEE 34-bus Feeder Data and BUVR Analysis

In this stage, the IEEE 34-bus feeder data (Configuration 300) has been listed in

Table 3.8, and the corresponding impedance has been expressed in (3.38) [57].

Table 3.8 – IEEE 34-bus feeder data (Configuration 300).

Phasing	Phase ACSR	Neutral ACSR	Spacing ID
B C A N	1/0	1/0	500

Phasing	Phase ACSR	Neutral ACSR	Spacing ID
B C A N	1/0	1/0	500

$$Z_{phase\_34-bus(\Omega/mi)} = \begin{bmatrix} 1.3368 + j1.3343 & 0.2101 + j0.5779 & 0.2130 + j0.5015 \\ 0.2101 + j0.5779 & 1.3238 + j1.3569 & 0.2066 + j0.4591 \\ 0.2130 + j0.5015 & 0.2066 + j0.4591 & 1.3294 + j1.3471 \end{bmatrix} \quad (3.38)$$

The above impedance matrix has been expressed based on the phase impedance. In order to express this matrix to sequences impedance the following equation is used:

$$Z_{012\_34-bus} = A^{-1} Z_{phase\_34-bus} A \quad (3.39)$$

Z_{012_34-bus} is translated to IEEE 30-bus feeder according to what discussed in section 3.2.4. In other words, based on Thevenin positive sequence impedance resulting from Z_{bus}, V_i from load flow analysis, and Z_{phase_34-bus}, sequences impedance for each feeder ($Z_{f,i}$ in Figure 3.4) is calculated by:

$$Z_{f,i} = \frac{Z_{f11,i}}{Z_{012\_34-bus}(2,2)} Z_{012\_34-bus}(2,2) \quad (3.40)$$

Where $Z_{f11,i}$is positive sequence impedance calculated by (3.30) and (3.31) and *i* corresponds to the bus number. This provides the way to calculate BUVR of the system based on the new feeder data. The results for BUVR has been shown in Figure 3.7. The results demonstrate that UVR for each bus is below the permissible limit of 3%, it and does not put risk on the system and the associating components in terms of power quality issues.

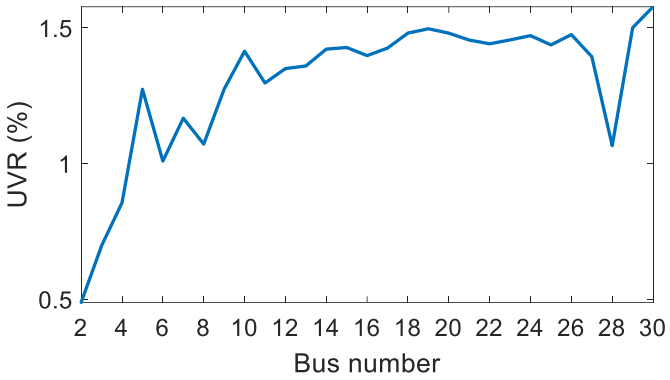

Figure 3.7– BUVR of system buses.

According to the obtained BUVR, maximum charging station capacity that could be connected to each bus subjected to (3.26) and (3.27) constrains is calculated. This means that a three phase load should be connected to bus *i* in Figure 3.4, and two terms should be added to (3.36) which yields to:

$$\begin{bmatrix} 1.06 - V_{1,i} \\ 0 - V_{2,i} \end{bmatrix} = \begin{bmatrix} Z_{f11,i} & Z_{f12,i} \\ Z_{f21,i} & Z_{f22,i} \end{bmatrix} \begin{bmatrix} \frac{V_{1,i}}{Z_{g11,i}} + I_{1,FCS} \\ \frac{V_{2,i}}{Z_{g11,i}} + I_{2,FCS} \end{bmatrix} \tag{3.41}$$

Where $I_{1,FCS}$ and $I_{2,FCS}$ are positive sequence and negative sequence current of the fast charging station. In order to solve equation (3.41), $I_{1,FCS}$ and $I_{2,FCS}$ should be expressed in terms of voltage. Obtaining $I_{1,FCS}$is straight forward and it can be calculated by the power equations, however, $I_{2,FCS}$is contingent upon negative sequence voltage. In order to express this current in terms of negative sequence voltage, Figure 2.21 is utilized such that the function which best fits the characteristic is extracted. This is done using MATALB curve fitting tool. Thus, $I_{1,FCS}$ and $I_{2,FCS}$ are expressed by:

$$I_{1,FCS} = \frac{P_{FCS}}{3V_{1,i}} \tag{3.42}$$

$$I_{2,FCS} = -0.00023230V_{2,i}^5 + 0.007092V_{2,i}^4 - 0.07226V_{2,i}^3 + 0.2209V_{2,i}^2 + 0.5094V_{2,i}^1 + 0.002003$$

Given that, the maximum fast charging station capacity and UVR for each bus has been shown in Figure 3.8 and Figure 3.9, respectively.

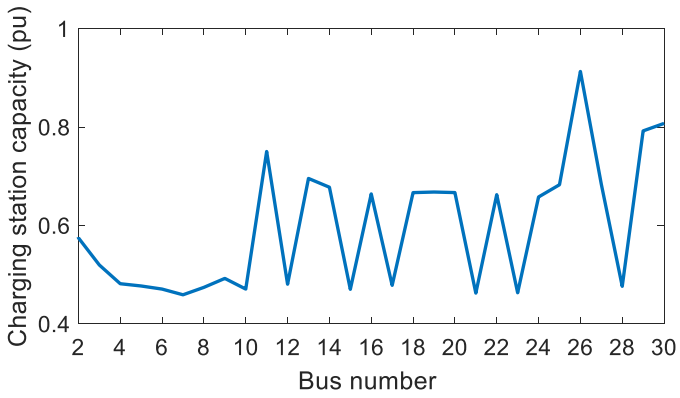

Figure 3.8– Maximum fast charging capacity.

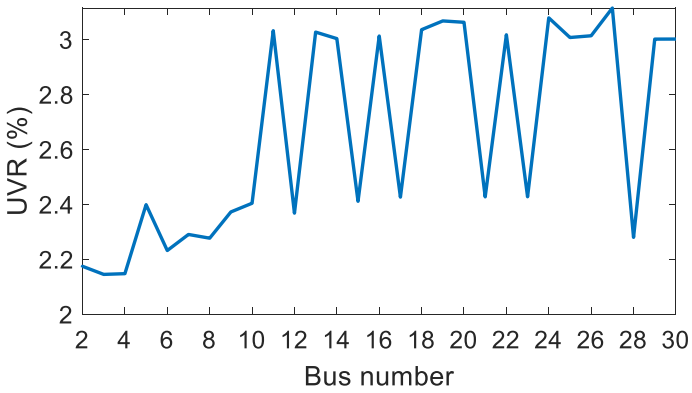

Figure 3.9– UVR after connection of fast charging station.

It is evident that some buses meet the maximum limit for UVR and for the rest, other constraints prevent that bus to host more charging capacity. The reason lies behind the fact that different buses have different sequences impedance which may lead to different situations.

3.2.4.3 IEEE 37-bus Feeder Data and BUVR Analysis

In this stage, the IEEE 37-bus feeder data (Configuration 721) has been listed in Table 3.9 and the corresponding impedance has been expressed in (3.43) [57].

Table 3.9 – IEEE 37-bus feeder data (Configuration 721).

Phasing	Cable	Spacing ID
A B C	1,000,000 AA, CN	515

$$Z_{phase\_37-bus(\Omega/mi)} = \begin{bmatrix} 0.2926 + j0.1973 & 0.0673 - j0.0368 & 0.0337 - j0.0417 \\ 0.0673 - j0.0368 & 0.2646 + j\,0.1900 & 0.0673 - j0.0368 \\ 0.0337 - j0.0417 & 0.0673 - j0.0368 & 0.2926 + j0.1973 \end{bmatrix} \quad (3.43)$$

The same procedure as described in section3.2.4.2 will be followed to obtain BUVR, maximum fast charging station capacity, and UVR after the connection of charging station. Figure 3.10 shows UVR of each bus before connection of any charging station. It is evident that bus number 30 has exceeded beyond the permissible level, thus it is expected that no charging station can be connected to this bus. Moreover, BUVR for this specific feeder is much higher than IEEE 34-bus feeder. One may conclude this is stemming from different configuration of the feeders which have been tested.

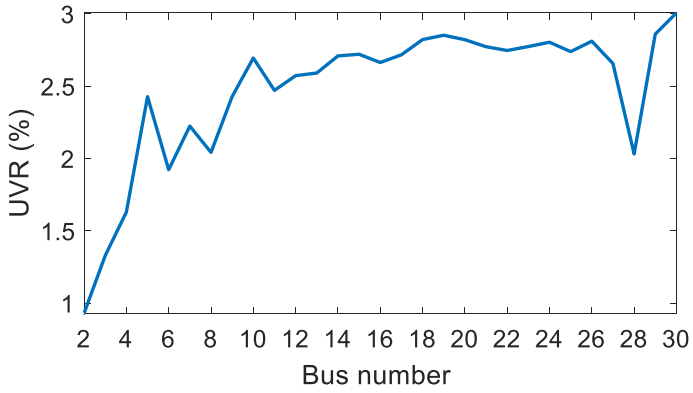

Figure 3.10– BUVR of system buses.

Figure 3.11 demonstrates maximum charging station capacity that can be integrated in the system at each bus. As it was expected the charging station capacity at bus number 30 is zero since BUVR at this bus was almost 3%. Moreover, due to high BUVR for this feeder comparing to IEEE 34-bus feeder, the maximum amount of the charging station capacity is significantly lower.

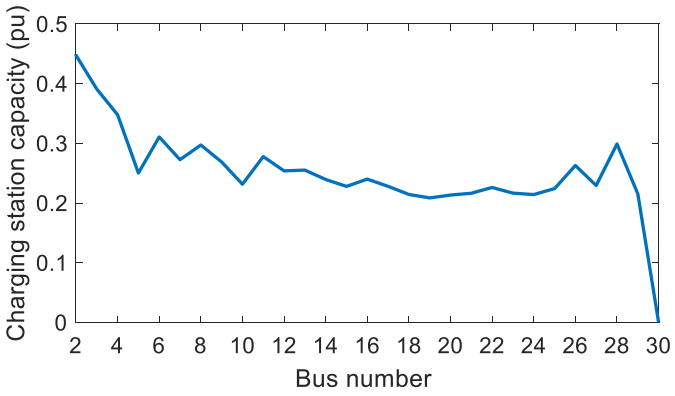

Figure 3.11– Maximum charging station capacity.

Figure 3.12 shows the UVR after connection of the charging station. It implies that the maximum capacity for charging station has been obtained until UVR constraint is met and the voltages of all buses are within the acceptable range and are not violated. It is worthy to mention that the utilized feeder in this section is cable while the one in the previous section was an overhead line feeder and it may lead to the differences between the results of these two sections.

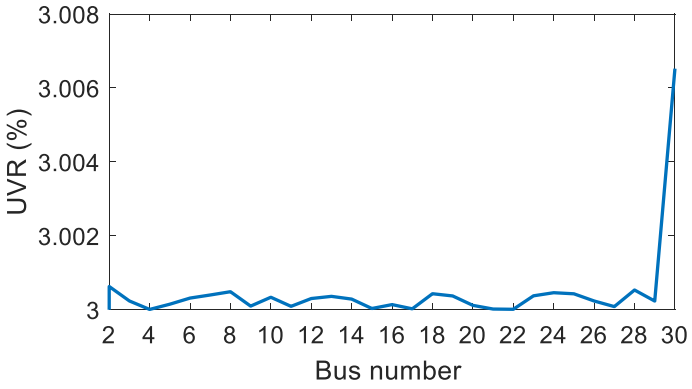

Figure 3.12– UVR after connection of charging station.

3.2.4.4 IEEE 123-bus Feeder data and BUVR analysis

In this stage, the IEEE 37-bus feeder data (Configuration 1) has been listed in Table 3.10 and the corresponding impedance has been expressed in (3.44) [57].

Table 3.10 – IEEE 123-bus feeder data (Configuration 1).

Phasing	Phase Cond. ACSR	Neutral Cond. ACSR	Spacing ID
A B C	336,400 26/7	4/0 6/1	500

$$Z_{phase\_123-bus(\Omega/mi)} = \begin{bmatrix} 0.4576 + j1.0780 & 0.1560 + j0.5017 & 0.1535 + j0.38497 \\ 0.1560 + j0.5017 & 0.4666 + j1.0482 & 0.1580 + j0.4236 \\ 0.1535 + j0.38497 & 0.1580 + j0.4236 & 0.4615 + j1.0651 \end{bmatrix} \quad (3.44)$$

The same procedure as described in section 3.2.4.2 will be followed to obtain BUVR, maximum fast charging station capacity, and UVR after the connection of charging station. Figure 3.13 shows UVR of system buses before connection of any charging station to the system. It is clear that buses number 29 and 30 go beyond permissible limit for UVR preventing system operator to integrate the charging station at these buses. Figure 3.14 shows maximum charging station capacity. Comparing Figure 3.13 and Figure 3.14 implies that the higher the BUVR, the less the charging capacity.

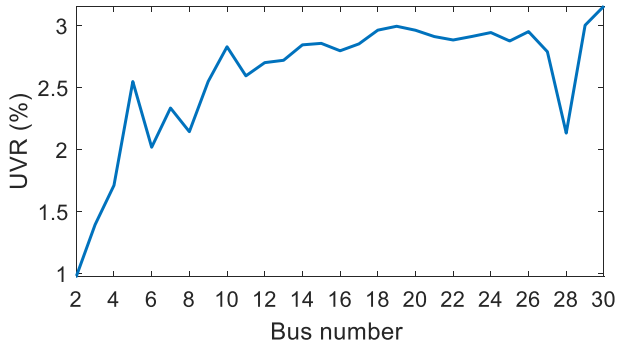

Figure 3.13– BUVR of system's buses.

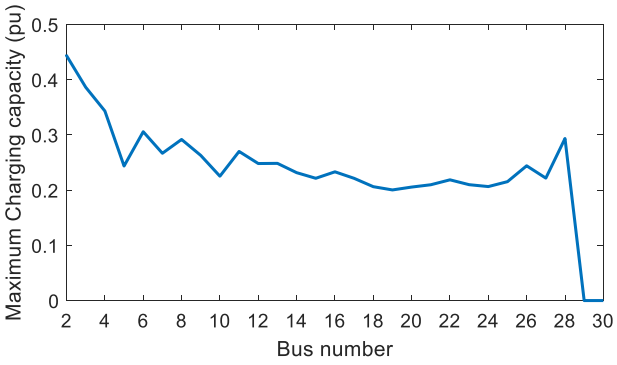

Figure 3.14– Maximum charging station capacity.

Figure 3.15 indicates that all buses reach the limit and their voltage is within the acceptable range. In the figure below UVR of bus number 29 and 30 have not been shown in order not to lose the resolution of the figure, however the corresponding UVR for bus number 29 and 30 are 3.004 and 3.16, respectively. The feeder used in this section is the overhead line feeder.

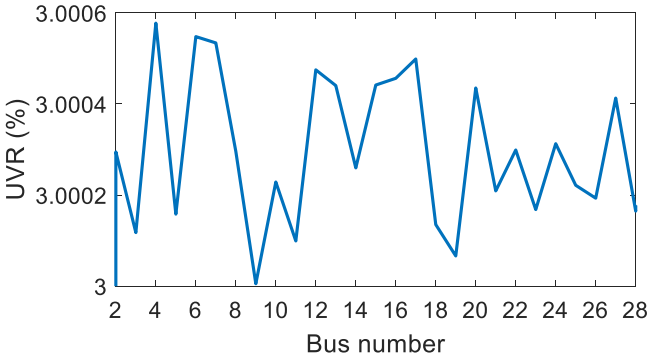

Figure 3.15– UVR of system buses after charging station connection.

Chapter 4 Mitigation Method

4.1 Introduction

In the previous chapter, it was investigated that the unbalanced voltage through the feeders is caused by the interaction of the phases leading to mutual impedance in all phases of the feeders. The increase of the negative sequence current would be an adverse and destructive consequence of this effect which prevents the integration of fast charging stations into the power system. In addition, since negative sequence component rotates at synchronous speed but in opposite direction of the positive sequence, it results in induction of double frequency current in rotor of the electrical machines and causes rapid heat increase. Increase in rotor temperature may lead to failure of insulation and loss of mechanical integrity [58]. These consequences are inevitable in the presence of negative sequence current. Thus a promising solution to reduce unbalanced voltage in the system is mitigating the effect of mutual impedances in the feeders. This not only neutralizes negative sequence current but also allows more connection of fast charging station in the system.

In order to eliminate the mutual impedance in feeders' impedance matrix, transposition of the feeders is a guaranteed way to follow. When the lines are transposed, the phases of the lines are displaced by their position counteracting their mutual effect on each other. Mutual impedances tends to zero only if the transposition is done completely. In other words, the feeder should be divided by three equal sections and the displacement should be done perfectly. But a complete transposition is not always feasible due to some limitations such as geographical features of the area, connection of the loads between the sections which changes the symmetry, etc. Thus in some occasions, partial transposition is carried out. Although, partial transposition does not completely eliminate the mutual impedances, it highly reduces their effect. In this chapter, a modified partial transposition is carried out such that it mitigates mutual impedance effect more than common partial transposition. The feeders' data of IEEE 34-bus, 37-bus, and

123-bus are partially transposed and implemented in IEEE 30-bus system, and maximum charging capacity that can be connected to the system due to partial transposition will be calculated. Then, in order to enhance power quality of the system, partial transposition is implemented by applying a modifying factor to off-diagonal elements of the impedance matrix such that the buses of the system will not experience more than 1 % BUVR while the buses are still subjected to voltage constraint. Then the modified transposed feeders' data will be employed to calculate maximum fast charging capacity, and the results will be compared with the previous analysis.

Eventually, a power distance table will be presented according to which fast charging station capacity will be expressed in term of electrical distance. In other words, in analogy with distance relay which operates based on the impedance of the line, power distance table is used to determine fast charging station capacity based on impedance of each bus from the main substation.

Power distance table can be used for meshed systems. Since these systems are interconnected, and in contrary to the radial networks the impedance of the buses do not change linearly. Thus, power distance table provides the ability for system operators for making better decision about the connection of the loads in the power grid without jeopardizing the system stability.

4.2 Line Transposition

This section describes the alternatives to mitigate the effect of mutual impedances of the feeders.

Suppose the three-phase line impedance shown in Figure 4.1. The length of the line is assumed to be per unit and mutual impedance of the ground has been neglected for sake of ease. z_{aa}, z_{bb}, and z_{cc} are self-impedance of each phase, and z_{ab}, z_{ac}, and z_{bc} are coupling or mutual-impedances.

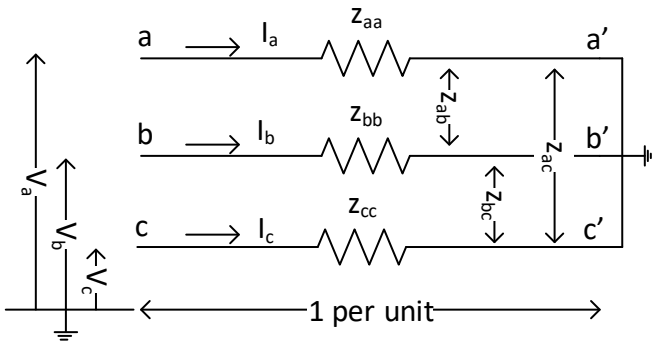

Figure 4.1– A three-phase line.

The voltage of each phase would be calculated by:

$$\begin{bmatrix} V_a \\ V_b \\ V_c \end{bmatrix} = \begin{bmatrix} z_{aa} & z_{ab} & z_{ac} \\ z_{ab} & z_{bb} & z_{bc} \\ z_{ac} & z_{bc} & z_{cc} \end{bmatrix} \begin{bmatrix} I_a \\ I_b \\ I_c \end{bmatrix} \text{ V/unit length} \tag{4.1}$$

It is clear from (4.1) that the voltage drop in each phase depends on the self and mutual impedances. The voltage drop for each phase might be different depending on configuration of the lines and conductors distance [59]. In other words, since mutual impedances are unequal, the voltage drop is unequal, as well. Thus in order to make mutual impedance equal to each other, transposition is suggested as a promising remedy. A transposition is physical displacement of conductors such that the conductors are changed by their physical position and moved to next physical position in a controlled manner like a-b-c, c-a-b, and b-c-a. If the line is divided into three equal segments and the conductors are transposed within each segment

according to the regular manner, this is called complete transposition. Figure 4.2 shows the transposition for a line.

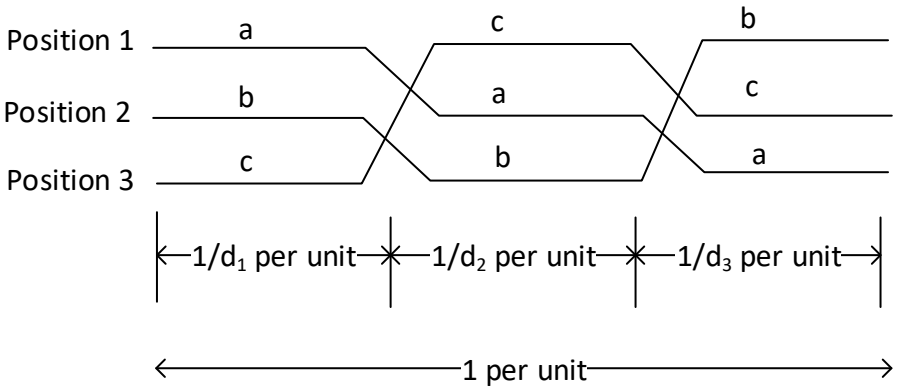

Figure 4.2– The transposition of a line.

In the above figure, the line has been divided to three section with different lengths. The impedance of each section would be defined as follows:

$$Z_{mn-s} = \frac{1}{d_s} Z_{mn} \tag{4.2}$$

Where, s=1, 2, or 3 is section indicator, m, n=1, 2, 3 indicating the position, $\frac{1}{d_s}$ is length of section s_{th}, and Z_{mn} is the total impedance corresponding to position m, n. thus voltage equation for each section can be obtained as follows:

For section 1, positions 1, 2, and 3 correspond to phase a, b, and c.

$$\begin{bmatrix} V_a \\ V_b \\ V_c \end{bmatrix} = \begin{bmatrix} V_1 \\ V_2 \\ V_3 \end{bmatrix} = \begin{bmatrix} z_{11-1} & z_{12-1} & z_{13-1} \\ z_{21-1} & z_{22-1} & z_{23-1} \\ z_{31-1} & z_{32-1} & z_{33-1} \end{bmatrix} \begin{bmatrix} I_a = I_1 \\ I_b = I_2 \\ I_c = I_3 \end{bmatrix} \text{ V/unit length} \tag{4.3}$$

For section 2, positions 1, 2, and 3 correspond to phase c, a, and b.

$$\begin{bmatrix} V_a \\ V_b \\ V_c \end{bmatrix} = \begin{bmatrix} V_2 \\ V_3 \\ V_1 \end{bmatrix} = \begin{bmatrix} z_{22-2} & z_{23-2} & z_{21-2} \\ z_{32-2} & z_{33-2} & z_{31-2} \\ z_{12-2} & z_{13-2} & z_{11-2} \end{bmatrix} \begin{bmatrix} I_a = I_2 \\ I_b = I_3 \\ I_c = I_1 \end{bmatrix} \text{ V/unit length} \tag{4.4}$$

And for section 3, positions 1, 2, and 3 correspond to phase b, c, and a.

$$\begin{bmatrix} V_a \\ V_b \\ V_c \end{bmatrix} = \begin{bmatrix} V_3 \\ V_1 \\ V_2 \end{bmatrix} = \begin{bmatrix} z_{33-3} & z_{31-3} & z_{32-3} \\ z_{13-3} & z_{11-3} & z_{12-3} \\ z_{23-3} & z_{21-3} & z_{22-3} \end{bmatrix} \begin{bmatrix} I_a = I_3 \\ I_b = I_1 \\ I_c = I_2 \end{bmatrix} \text{ V/unit length} \tag{4.5}$$

Thus the total voltage would be equal to summation of (4.3), (4.4), and (4.5):

$$\begin{bmatrix} V_{at} \\ V_{bt} \\ V_{ct} \end{bmatrix} = \begin{bmatrix} (z_{11-1} + z_{22-2} + z_{33-3}) & (z_{12-1} + z_{23-2} + z_{31-3}) & (z_{13-1} + z_{21-2} + z_{32-3}) \\ (z_{21-1} + z_{32-2} + z_{13-3}) & (z_{22-1} + z_{33-2} + z_{11-3}) & (z_{23-1} + z_{31-2} + z_{12-3}) \\ (z_{31-1} + z_{12-2} + z_{23-3}) & (z_{32-1} + z_{13-2} + z_{21-3}) & (z_{33-1} + z_{22-3} + z_{22-3}) \end{bmatrix} \begin{bmatrix} I_a \\ I_b \\ I_c \end{bmatrix} \text{ V/unit length} \tag{4.6}$$

Substituting for Z_{mn-s} of (4.2) in (4.6) yields:

$$\begin{bmatrix} V_{at} \\ V_{bt} \\ V_{ct} \end{bmatrix} = \begin{bmatrix} (\frac{1}{d_1}z_{11} + \frac{1}{d_2}z_{22} + \frac{1}{d_3}z_{33}) & (\frac{1}{d_1}z_{12} + \frac{1}{d_2}z_{23} + \frac{1}{d_3}z_{31}) & (\frac{1}{d_1}z_{13} + \frac{1}{d_2}z_{21} + \frac{1}{d_3}z_{32}) \\ (\frac{1}{d_1}z_{21} + \frac{1}{d_2}z_{32} + \frac{1}{d_3}z_{13}) & (\frac{1}{d_1}z_{22} + \frac{1}{d_2}z_{33} + \frac{1}{d_3}z_{11}) & (\frac{1}{d_1}z_{23} + \frac{1}{d_2}z_{31} + \frac{1}{d_3}z_{12}) \\ (\frac{1}{d_1}z_{31} + \frac{1}{d_2}z_{12} + \frac{1}{d_3}z_{23}) & (\frac{1}{d_1}z_{32} + \frac{1}{d_2}z_{13} + \frac{1}{d_3}z_{21}) & (\frac{1}{d_1}z_{33} + \frac{1}{d_2}z_{22} + \frac{1}{d_3}z_{22}) \end{bmatrix} \begin{bmatrix} I_a \\ I_b \\ I_c \end{bmatrix} \text{ V/unit length} \tag{4.7}$$

It is clear that for similar conductors $Z_{11}= Z_{22}= Z_{33}= Z_s$, and since the network is considered to be linear $Z_{mn}= Z_{nm}$. Thus (4.7) can be written as:

$$\begin{bmatrix} V_{at} \\ V_{bt} \\ V_{ct} \end{bmatrix} = \begin{bmatrix} Z_s & Z_{M1} & Z_{M2} \\ Z_{M1} & Z_s & Z_{M3} \\ Z_{M2} & Z_{M3} & Z_s \end{bmatrix} \begin{bmatrix} I_a \\ I_b \\ I_c \end{bmatrix} \text{ V/unit length} \tag{4.8}$$

It is apparent from (4.7), if the sections are equally divided, off-diagonal elements of impedance matrix of (4.8) will be equal. The line would be completely transposed under this circumstance which leads to:

$$\begin{bmatrix} V_{at} \\ V_{bt} \\ V_{ct} \end{bmatrix} = \begin{bmatrix} Z_s & Z_M & Z_M \\ Z_M & Z_s & Z_M \\ Z_M & Z_M & Z_s \end{bmatrix} \begin{bmatrix} I_a \\ I_b \\ I_c \end{bmatrix} \text{ V/unit length} \tag{4.9}$$

It is worth to mention that the above equation has been written based on phases abc, however power solution which were used in the previous chapter for determination of the maximum charging station were based on symmetrical sequences. Therefore, in terms of symmetrical sequences (4.9) can be calculated by [60]:

$$Z_{012} = A^{-1} Z_{abc} A \tag{4.10}$$

Where A is matrix defined in A.1. Therefore:

$$\begin{bmatrix} V_0 \\ V_1 \\ V_2 \end{bmatrix} = \begin{bmatrix} Z_0 & 0 & 0 \\ 0 & Z_1 & 0 \\ 0 & 0 & Z_2 \end{bmatrix} \begin{bmatrix} I_0 \\ I_1 \\ I_2 \end{bmatrix} \tag{4.11}$$

Where

$$\begin{aligned} Z_0 &= Z_s + 2Z_M \\ Z_1 &= Z_2 = Z_s - Z_M \end{aligned} \tag{4.12}$$

It is evident from (4.11), that the mutual impedances are zero. Therefore in this case, negative sequence voltage will not impose detrimental impacts on the power system and will not restrict connection fast charging station. However, a complete transposition is not always practical due to geographical features of the area, loading connection, etc.

So, one may conclude that in order to mitigate mutual impedances, partial transposition could be a viable solution. A partial transposition is defined as whether unequal division of line segments in one cycle or only transposing in c-a-b or b-a-c sequences.

4.3 Methodology

It was deduced from the previous section that the partial transposition could be a potential way to reduce mutual impedance. In this section, partial transposition and modified partial transposition are conducted and the results will be compared.

4.3.1 Partial transposition

IEEE 34-bus, 37-bus, and 123-bus feeders would be partially transposed such that the transposition is done only for c-a-b sequence and the length of the two sections are equal. This is conducted by using phase impedances of each feeder mentioned in section 3.2.4 and equations (4.3), (4.4), and (4.10). The partial transposition for this method has been shown in Figure 4.3. Then based on the obtained values for each benchmark the maximum capacity for charging station will be obtained for the studied system (IEEE 30-bus benchmark) while the system is subjected to UVR and voltage constraints.

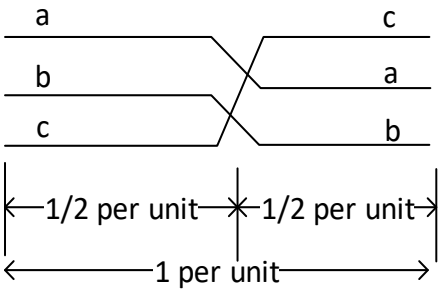

Figure 4.3– Partial transposition of the feeder.

For IEEE 34-bus feeder's data, Figure 4.4, Figure 4.5, and Figure 4.6 show BUVR, the maximum charging station capacity, and UVR after and before partial transposition for each bus, respectively.

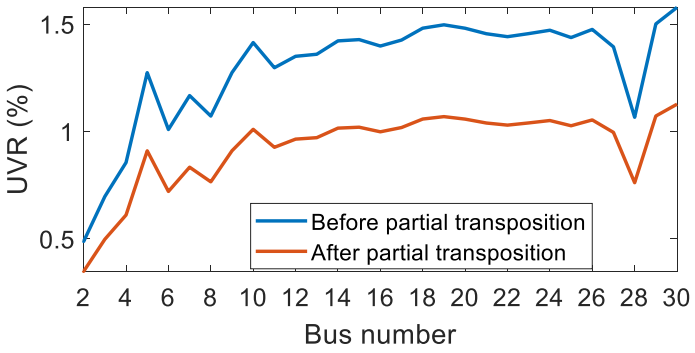

Figure 4.4– BUVR of the system before and after partial transposition.

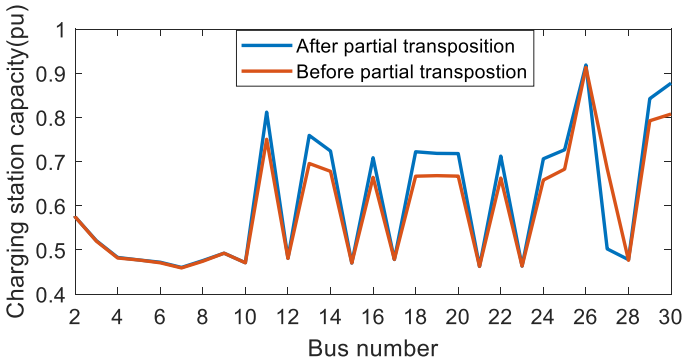

Figure 4.5– Maximum fast charging station capacity before and after partial transposition.

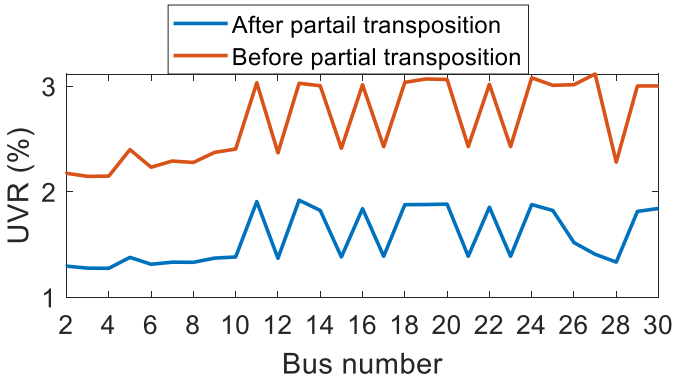

Figure 4.6– UVR of the system after and before partial transposition and after connection of charging stations.

The above figures imply that BUVR of the system after partial transposition is within the acceptable range (BUVR < 1.1%) providing safe operation for the power system in terms of power quality. Moreover, the maximum capacity for charging stations have been obtained while the UVR of the system is well below permissible limit (3%). This means that there would be safe margin if other loads undergo unbalanced conditions in addition to the fast charging station. Figure 4.6 proves that partial transposition facilitates integration of the fast charging station by partially eliminating the impacts of mutual impedances.

For IEEE 37-bus feeder's data, Figure 4.7, Figure 4.8, and Figure 4.9 show BUVR of the system after partial transposition, the maximum charging station capacity and UVR after partial transposition for each bus, respectively. The Figure 4.7 indicates that BUVR of the system is less than 1.5 %. It is mandatory to investigate UVR of the system after connection of charging station. If UVR touches the upper limit, it means that partial transposition is not a reliable solution for this feeder. Furthermore, the maximum charging capacity has been obtained while most of the buses of system have touched the maximum limit for UVR (3 %). For those buses which do not suffer from high UVR, the limiting factor is the voltage constraint. Although the capacity of the charging station can be increased compared with the non-transposed feeders, it can be concluded that for this particular feeder, partial transposition with equal segments is not an effective solution, since it does not provide a secure margin for future development of the system.

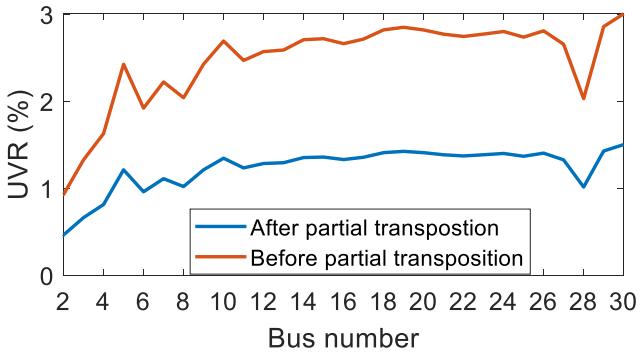

Figure 4.7– BUVR of the system after and before partial transposition.

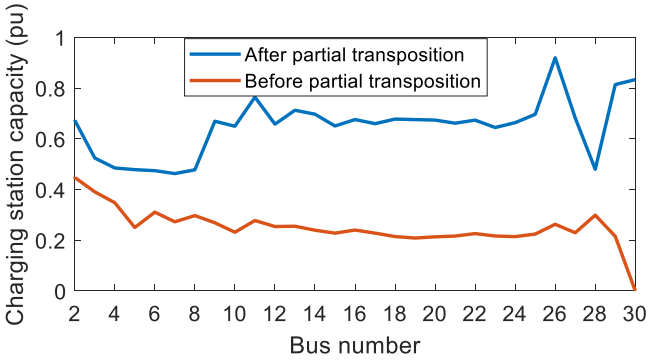

Figure 4.8– Maximum fast charging station capacity after and before partial transposition.

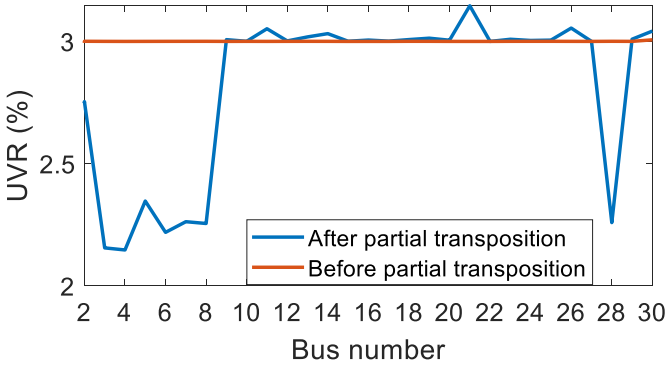

Figure 4.9– UVR of the system after and before partial transposition and after connection of charging stations.

For IEEE 123-bus feeder's data, conducting the same analysis, one may deduce from the Figure 4.10 to Figure 4.12 that the BUVR has been decreased, and the charging capacity has been increased compared to the non-transposed feeder. Similar to the other figures, the restricting factor for some buses is UVR and for the others is the voltage constraint. As mentioned for

IEEE 37-bus feeder, since some buses are limited by UVR, integration of extra loads to this buses is not feasible, thus a safe alternative should be taken into consideration to hinder the increase of UVR due to integration of fast charging stations.

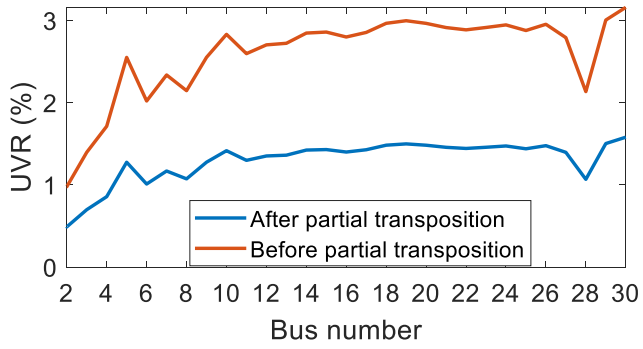

Figure 4.10– BUVR of the system after and before partial transposition.

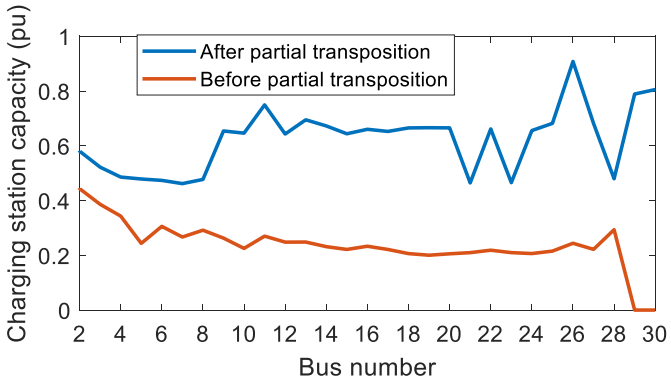

Figure 4.11– Maximum fast charging station capacity after and before partial transposition.

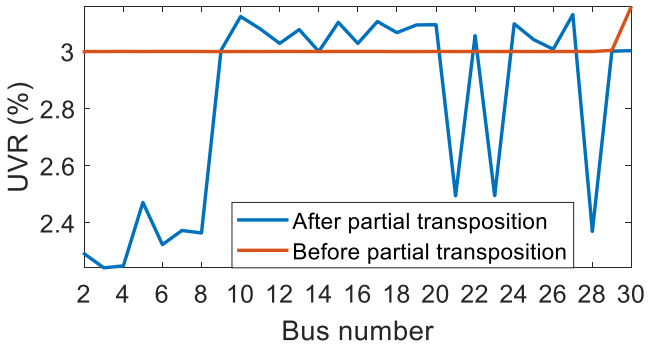

Figure 4.12– UVR of the system after and before partial transposition and after connection of charging stations.

4.3.2 Modified Partial Transposition

In the previous section the data for three different feeders were implemented in the studied system, and UVR analysis were done for partial transposition of the feeders. It was demonstrated that the IEEE 34-bus feeder's partial transposition responded appropriately, and the UVR for each bus was well below the acceptable limit. As for other two feeders (in IEEE 37-bus and 123-bus benchmark systems), the results showed that despite the partial transposition, UVR for some buses meets the limit and it keeps the system within bounds and hampers the connection of additional. In other words, for some feeders, partial transposition is still a flawed method. Accordingly, another approach should be adopted to compensate for this deficiency. This would be encouraging to investigate the contributing factors for calculation of line impedance, especially mutual impedance of the line.

Mutual impedance can be calculated by equation [54]:

$$Z_{ab} = j\omega 2 \times 10^{-7} \left(\ln \frac{2s}{D_m} - 1 \right) \text{ H/ unit length} \tag{4.13}$$

The same equation can be used for Z_{ac} and Z_{bc}. Mutual impedance depends on length of the line section and D_m which is calculated by:

$$D_m = \sqrt[3]{D_{ab} D_{ac} D_{bc}} \text{ m} \tag{4.14}$$

Thus in each section of a transposed line these two factors can be manipulated such that it creates the least mutual impedance. Therefore, (4.13) can be rewritten as:

$$Z_{ab} = j\omega 2 \times 10^{-7} \alpha_m \left(\ln \frac{2s'}{D_m'} - 1 \right) \text{ H/ unit length} \tag{4.15}$$

Where α_m is the modifying factor. This factor is applied to off-diagonal elements of equation (3.34). Having done that, Newton-Raphson algorithm is used to solve (3.34) and find modifying factor for the different IEEE feeders' data such that the corresponding BUVR would be set to 1 %. The reason for this assumption has its roots in some restrictions which prevents complete transposition. In addition to UVR constraint, voltage constraint is taken into

consideration. In this case the lower limit remains the same value but the upper limit is turned to be the voltages listed in Table 3.3 where the voltages are calculated when the system is operating in normal conditions and without connection of any additional load or generation. The modified transposition is applied to IEEE 37-bus and 123-bus feeders due to their high BUVR (more than 1%) after partial transposition. Then, the maximum capacity for charging station would be obtained while the system is subjected to UVR and voltage constraint.

For IEEE 37-bus the results are as follows after the modified transposition. Figure 4.13 demonstrates that after connection of fast charging station with maximum capacity, there is a good marginal safety for system functioning in terms of UVR.

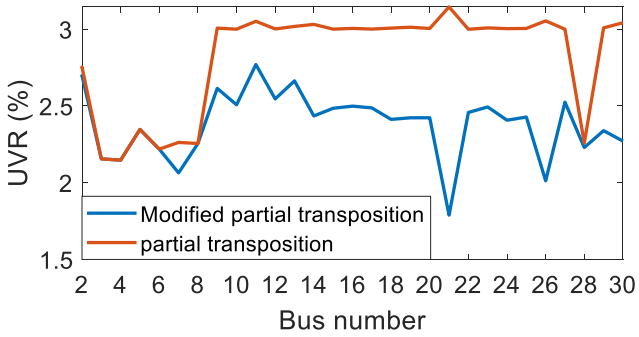

Figure 4.13– UVR of the system after modified transposition and charging station integration.

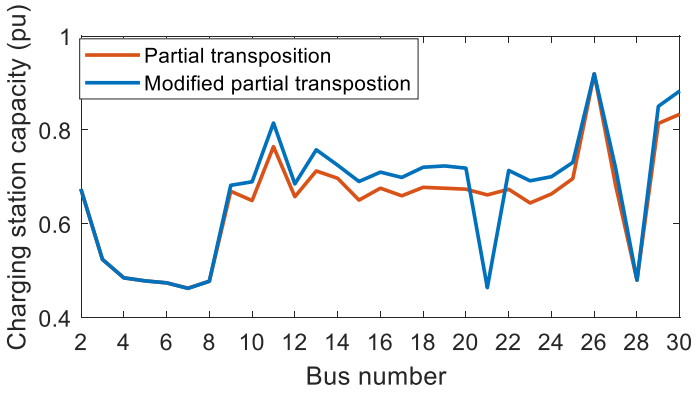

Figure 4.14– Comparison of fast charging station capacity between partial transposition and modified transposition.

Figure 4.14 proves that the modified transposition not only allows for connection of higher capacity fast charging stations but also maintains the UVR of the system below the maximum

acceptable level. Another remarkable fact about the results is that for bus number 21 since initial UVR (BUVR) for this bus was set to be 1 % and after connecting the fast charging station, the UVR reaches around 1.75 % which is less than the other buses, it conveys that the voltage constraint is the dominant limiter for this specific bus and it causes less integration compered to the partial transposition case.

For IEEE 123-bus feeder the following results are remarkable. Figure 4.15 shows the UVR of the system after the modified transposition. It implies that the UVR does not exceed the limit. So the voltage constraint is dominant to choose the maximum charging capacity.

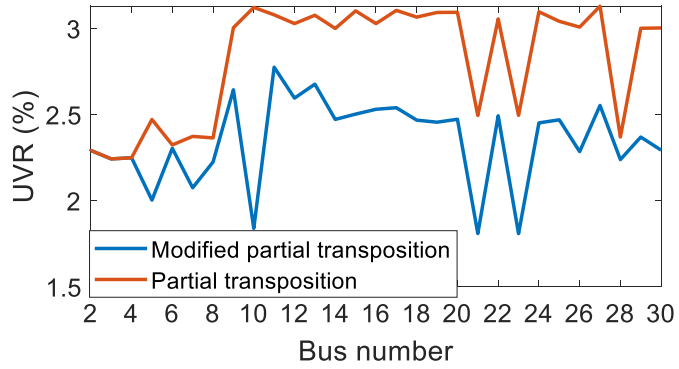

Figure 4.15– UVR of the system after modified transposition.

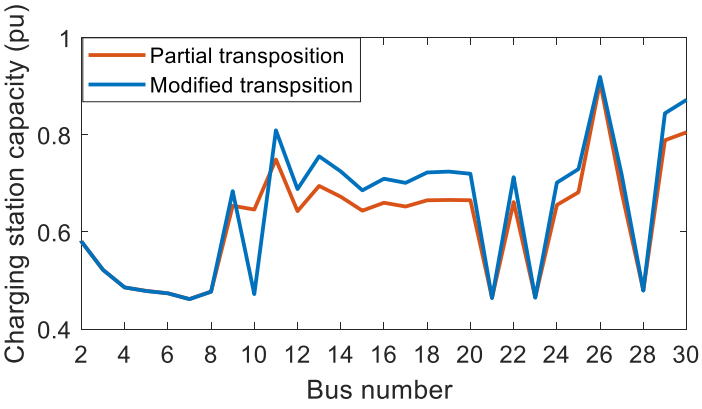

Figure 4.16– Comparison of fast charging station capacity between partial transposition and modified transposition.

Figure 4.16 shows the capacity can be increased due to the modified transposition.

This section showed that the modified transposition is a promising way that can be relied on. Power quality of the system can be provided through this method. Moreover, it was shown that this approach is a comprehensive one since it includes different feeders with different data.

4.4 Power Distance Table

In this thesis, power distance table is defined as a tool to express maximum fast charging capacity that can be connected to the system in terms of electrical distance (impedance) of the installation point to the main substation. This method is analogous to distance relays which are tuned based on electrical distance (impedance) of the transmission line and operate during occurrence a fault whose impedance is less than the tuned value. This approach provides a fast and effective way for utilities to have a better insight about resiliency of the system when fast charging stations are connected. Moreover, it is applicable for both radial and mesh systems. For instance, based on impedance and corresponding bus information, one may estimate the amount of load that can be connected to the system looking up in the power distance table. The results of the previous investigations has been listed in Table 4.1. According to this table, the maximum capacity that can be connected to the system will be obtain based on the connection point distance from the main source. Table below provides the information about the investigated feeders' data. As an example, for IEEE 34-bus feeder data, the maximum capacity charging station for any distance between the provided values in the table can be obtained. In order to obtain power distance table for any other power system, the same analysis should be conducted. Thus, the distance of the feeders and bus information such as load's type and level determine the maximum capacity for the new power system.

Table 4.1 – Power distance table.

Distance (km)	34-bus (MW)	37-bus (MW)	123-bus (MW)
2.033752	91.88	91.94	91.95
2.059	87.76	88.3	87.22

2.1206	84.26	85.04	84.45
2.388	81.2	81.48	80.95
2.43153	72.68	73.08	72.95
2.45078	50.24	71.88	71.78
2.5034	47.73	47.84	47.83
2.5142	71.86	72.33	72.44
2.523	72.23	72.05	72.26
2.5288	71.86	71.86	72.44
2.538	46.04	46.24	46.16
2.54	75.94	75.78	75.59
2.54272	52.1	52.42	52.2
2.5488	70.64	70.04	70.17
2.558	71.25	71.37	71.29
2.56053	47.59	47.76	47.69
2.5618	72.4	72.49	72.48
2.5638	47.8	47.99	47.92
2.5645	57.51	67.32	58.04
2.565	48.3	48.49	48.58
2.59	70.88	71.01	70.97
2.6	47.22	47.42	47.37

2.61	47.83	69.88	70.12
2.626	46.34	69.16	46.46
2.6279	49.27	68.2	68.42
2.628	46.27	46.4	46.38
2.6475	47.03	69.01	68.58
2.6592	47.11	68.95	47.2
2.7011	48.11	68.49	68.83

Chapter 5 Contributions and Future works

5.1 Contributions and conclusions

In this thesis, a comprehensive study of the effects of fast charging station on the IEEE 30-bus system using different feeders' data was conducted. The investigation includes power quality issues that the charging station may create such as UVR of the system. Thus, obtaining the fast charger behaviour under unbalanced input voltage was inevitable.

Chapter 2 was dedicated for deriving this characteristic. In this chapter, a fast charger was designed and developed. A boost PFC AC/DC converter followed by a Buck DC/DC converter formed that charger. The simulation results showed that the rectifier operates with unity power factor and provides a desired voltage at the output. The DC/DC converter functions with CC-CV charging scheme and appropriately delivers the power to the battery based on the designed procedure.

In order to capture the input current waveform of the charger under unbalanced condition, an unbalanced voltage was applied to the charger. The applied voltage contained negative sequence component in the range of 0-10 % of the positive sequence. During the unbalanced conditions, the THD of the input current was calculated and compared with the normal (only positive sequence) condition. The results demonstrated that during the normal operation, THD of the input current does not exceed the corresponding permissible limit, however, the unbalanced voltage input results in high harmonic contents in the input current. In this case, the negative sequence current characteristic was derived in terms of negative sequence voltage and it is used in chapters 3 and 4 for power flow analysis. This characteristic is employed to determine the amount of the fast charging capacity that could be connected to the system without violating the power quality and the voltage regulation in the power system.

In Chapter 3, the IEEE 30-bus benchmark system underwent a power quality investigation. Various feeder configurations from different benchmarks such as IEEE 34-bus, 37-bus and 123-bus were selected to adopt in the studied benchmark and conduct a comprehensive study of the fast charging station impacts on the system UVR. These feeders include both overhead line and cables making the study more complete and rigorous.

This chapter showed that the negative sequence voltage which results in the power quality issues may rise due to the unbalanced feeder configurations. In order to calculate positive and negative sequence voltage, two functions were developed based on the positive and negative sequence voltages and solved with Newton-Raphson algorithm. Examination of different feeders showed the fact that based on the various feeder configurations and the associating impedances, different UVR values will be obtained. This can limit the integration of more loads into the power system. It was observed that for the IEEE 37-bus and IEEE 123-bus feeders, UVR was a significant restriction for the integration of the fast charging stations. In the case of the IEEE 34-bus feeder, in addition to UVR limit, voltage constraint limited the integration of the charging station, as well. However, since the BUVR for this feeder was less than the other two cases, more capacity was allowed to be connected. Indeed, UVR has its roots in mutual sequence impedances caused by interaction of the three phases. In order to neutralize this effect and enable more connection of the fast charging stations, a solution is needed to be taken into consideration.

Chapter 4 introduced a mothed to reduce the mutual impedance effects. The employed approach is the partial and the modified transpositions. It was mentioned that due to some restrictions in some places, a complete transposition which utterly damps the mutual impedance effect is not feasible. Thus partial and modified transpositions would be appropriate solutions. It was demonstrated that for the IEEE 34-bus feeder, the BUVR of the system is less than 1 % (for some buses close to 1 %) only with adoption of the partial transposition, and after connection of the fast charging station with their maximum capacity the UVR remains well below the acceptable limit (3 %). On the other hand, as for the IEEE 37-bus and 123-bus systems, the BUVR was within the acceptable range but with connection of the charging station, the dominant constraint that prevented from more connection was the UVR. Thus, in

these cases, a modified partial transposition approach was introduced to further mitigate the effect of the unbalanced mutual impedances. In this approach, the distance between the phase conductors and the length of each feeder section, which mutual impedance relies on, were varied by a modifying factor. Then, implementing the modifying factor in the Newton-Raphson algorithm, developed in Chapter 3, the value of modifying factor would be obtained such that the BUVR is set to be 1 %. The simulation results demonstrated the effectiveness of this method. It was shown that the charging station capacity increased without UVR touching the upper limit value. In other words, the voltage constraint was the dominant one which prevented more connection of the charging station.

Eventually, power distance tables for the studied feeders were developed and presented in Chapter 4. From these plots, the power system planners are able to estimate additional loads (in this thesis, the charging station) that can be connected to the system based on the Thevenin impedance of the bus and the associating information such as the existing loads.

5.2 Future works

Regarding the increasing acceptance of PEVs in power grid and consequently the stochastic behaviour of PEV's drivers, it is highly crucial to conquer the challenges that PEVs and charging stations may impose on power systems. Moreover, the important role of the renewable energies in power system should not be ignored, since these natural sources of energy can be utilized to counteract the adverse effect of charging stations and PEVs. Hence, future work may include the following:

- Profound investigation of li-ion batteries characteristic for increasing the mile range of PEVs. The batteries should be modeled precisely in the simulations, in order to avoid loss of accuracy in practical experiments.
- Integration of renewable energies along with charging stations and consideration of PEV drivers' behavior. Coordination between the charging stations and renewable energies can mitigate the adverse effect of charging station on power system.

- Investigating the effect of ultrafast charging station on power system. One of the ways to reduce charging duration is using ultrafast chargers. But theses chargers impose detrimental effects on power system due to high power consumption. Thus, it is important to study the behaviour of ultrafast charging stations while they are connected to the system and operating under both normal and abnormal condition.

References

[1] S. Habib and S. Member, “A Comprehensive Study of Implemented International Standards , Technical Challenges , Impacts and Prospects for Electric Vehicles,” *IEEE Access*, vol. 6, pp. 13866–13890, 2018.

[2] Q. Yan, S. Member, B. Zhang, S. Member, M. Kezunovic, and L. Fellow, “Optimized Operational Cost Reduction for an EV Charging Station Integrated With Battery,” *IEEE Trans. Smart Grid*, vol. 10, no. 2, pp. 2096–2106, 2019.

[3] Z. Ding, Y. Lu, S. Member, L. Zhang, W. Lee, and D. Chen, “A Stochastic Resource-Planning Scheme for PHEV Charging Station Considering Energy Portfolio,” *IEEE Trans. Ind. Appl.*, vol. 54, no. 6, pp. 5590–5598, 2018.

[4] S. Murtaza and A. Shah, “Comparison of Characteristics - Lead Acid , Nickel Based , Lead Crystal and Lithium Based Batteries,” *2015 17th UKSim-AMSS Int. Conf. Model. Simul.*, pp. 444–450, 2015.

[5] J. Ahn, B. K. Lee, and S. Member, “High-Efficiency Adaptive-Current Charging Strategy for Electric Vehicles Considering Variation of Internal Resistance of Lithium-Ion Battery,” *IEEE Trans. Power Electron.*, vol. 34, no. 4, pp. 3041–3052, 2019.

[6] D. Baek and N. Chang, “Runtime Power Management of Battery Electric Vehicles for Extended Range With Consideration of Driving Time,” *IEEE Trans. Very Large Scale Integr. Syst.*, vol. 27, no. 3, pp. 549–559, 2019.

[7] Y. Shi, H. D. Tuan, A. V Savkin, T. Q. Duong, S. Member, and H. V. Poor, “Model Predictive Control for Smart Grids With Multiple Electric-Vehicle Charging Stations,” *IEEE Trans. Smart Grid*, vol. 10, no. 2, pp. 2127–2136, 2019.

[8] J. C. Mukherjee and A. Gupta, “A Review of Charge Scheduling of Electric Vehicles in Smart Grid,” *IEEE Syst. J.*, vol. 9, no. 4, pp. 1541–1553, 2015.

[9] Y. Zheng, Y. Song, and D. J. Hill, “Online Distributed MPC-Based Optimal Scheduling for EV Charging Stations in,” *IEEE Trans. Ind. Informatics*, vol. 15, no. 2, pp. 638–649, 2019.

[10] R. Energy and J. Contreras, “Impact of Electric Vehicles on the Expansion Planning of Distribution Systems Considering Charging Stations,” *IEEE Trans. Smart Grid*, vol. 10, no. 1, pp. 794–804, 2019.

[11] Y. Cheng, W. Wang, Z. Ding, and Z. He, “Electric bus fast charging station resource planning considering load aggregation and renewable integration,” vol. 13, pp. 1132–1141, 2019.

[12] M. Kefayati and C. Caramanis, “Efficient Energy Delivery Management for PHEVs,” *2010 First IEEE Int. Conf. Smart Grid Commun.*, no. i, pp. 525–530, 2010.

[13] R. Dufo-lópez *et al.*, “Multi-objective optimization minimizing cost and life cycle emissions of stand-alone PV – wind – diesel systems with batteries storage,” vol. 88, pp. 4033–4041, 2011.

[14] M. mainul Islam, H. Shareef, and A. Mohamed, “Optimal location and sizing of fast charging stations for electric vehicles by incorporating traffic and power networks,” pp. 947–957, 2018.

[15] S. Negarestani, M. Fotuhi-firuzabad, M. Rastegar, and A. Rajabi-ghahnavieh, “Optimal Sizing of Storage System in a Fast Charging Station for Plug-in Hybrid Electric Vehicles,” *IEEE Trans. Transp. Electrif.*, vol. 2, no. 4, pp. 443–453, 2016.

[16] O. Erdinç, S. Member, and A. Ta, “Comprehensive Optimization Model for Sizing and Siting of DG Units , EV Charging Stations , and Energy Storage Systems,” vol. 9, no. 4, pp. 3871–3882, 2018.

[17] V.-L. Nguyen, T. Tran-Qyoc, and S. Bacha, “Harmonic Distortion Mitigation for Electric Vehicle Fast Charging Systems,” 2013, pp. 16–20.

[18] A. Pan, Y. Zhu, L. Ren, T. Chen, S. Wen, and W. Yun, “Harmonic Research of Electric Vehicle Fast Chargers,” in *2016 IEEE PES Asia-Pacific Power and Energy Engineering Conference (APPEEC)*, 2016, pp. 2545–2549.

[19] Y. Peng, J. Huang, Y. Li, P. Liu, and J. Cao, “A Novel Harmonic Detection Algorithm for Electric Vehicle with Charging Piles,” in *2018 IEEE 7th Data Driven Control and Learning Systems Conference (DDCLS)*, 2018, pp. 836–840.

[20] K. H. Shafad, J. J. Jamian, and S. A. S. Nasir, “Harmonic Distortion Mitigation for Multiple Modes Charging Station via Optimum Passive Filter Design,” in *2016 IEEE Conference on Systems, Process and Control (ICSPC)*, 2016, no. December, pp. 219–223.

[21] B. Arbsalmanabadi, A. Javadi, and K. Al-Haddad, “Analyzing Fast Charger in the Smart Grid from Power Quality’s Prospecting,” in *IECON 2017 - 43rd Annual Conference of the IEEE Industrial Electronics Society*, 2017, pp. 888–892.

[22] S. Alshareef and W. Morsi, “Impact of Fast Charging Stations on the Voltage Flicker in the Electric Power Distribution Systems,” in *2017 IEEE Electrical Power and Energy Conference (EPEC)*, 2017.

[23] B. Pea-da and S. Dechanupaprittha, “Impact of Fast Charging Station to Voltage Profile in Distribution System,” in *Proceedings of the International Electrical Engineering Congress 2014*, 2014, pp. 3–6.

[24] K. Clement-nyns, E. Haesen, S. Member, and J. Driesen, “The Impact of Charging Plug-In Hybrid Electric Vehicles on a Residential Distribution Grid,” vol. 25, no. 1,

pp. 371–380, 2010.

[25] Y. Liu, T. Chang, H. Chen, T. Chang, and P. Lan, “Power Quality Measurements of Low-Voltage Distribution System with Smart Electric Vehicle Charging Infrastructures,” *2014 16th Int. Conf. Harmon. Qual. Power*, pp. 631–635, 2014.

[26] T. Boonraksa, A. Paudel, P. Dawan, and B. Marungsri, “Impact of Electric Bus Charging on the Power Distribution System a Case Study IEEE 33 Bus Test System,” *2019 IEEE PES GTD Gd. Int. Conf. Expo. Asia (GTD Asia)*, pp. 819–823, 2019.

[27] C. Chan, H. Liou, and C. Lu, “Operation of Distribution Feeders with Electric Vehicle Charging Loads,” in *2012 IEEE 15th International Conference on Harmonics and Quality of Power*, 2012, pp. 695–700.

[28] R. Yan, T. K. Saha, and S. Member, “Investigation of Voltage Imbalance Due to Distribution Network Unbalanced Line Configurations and Load Levels,” *IEEE Trans. Power Syst.*, vol. 28, no. 2, pp. 1829–1838, 2013.

[29] M. Stenseth, R. Mushimiye, J. H. Poulsen, and M. Vadstrup, “Analysis of Model Simplification for a System Imposed by Voltage Unbalance Generated by Electric Trains,” *2018 53rd Int. Univ. Power Eng. Conf.*, pp. 1–6, 2018.

[30] D. R. Pinto *et al.*, *Field Investigation of the Power Quality Impact of Electric Vehicles in Secondary Residential Systems*. IEEE, 2018.

[31] M. Yilmaz and P. T. Krein, “Review of Battery Charger Topologies, Charging Power Levels, and Infrastructure for Plug-In Electric and Hybrid Vehicles,” *IEEE Trans. POWER Electron.*, vol. 28, no. 5, pp. 2151–2169, 2013.

[32] L. Yongxiang, H. Fuhui, X. Ruilin, C. Tao, X. Xin, and L. Jie, “Investigation on the construction mode of the charging station and battery-exchange station,” in *2011 Asia-Pacific Power and Energy Engineering Conference*, 2011, pp. 1–2.

[33] “Electric Vehicle Infrastructure Installation Guide.” Pacific Gas and Electric

Company, San Francisco, CA, USA, 1999.

[34] W. Su, H. Eichi, W. Zeng, and M. Chow, “A Survey on the Electrification of Transportation in a Smart Grid Environment,” *IEEE Trans. Ind. Informatics*, vol. 8, no. 1, pp. 1–10, 2012.

[35] N. Shaukat *et al.*, “A survey on electric vehicle transportation within smart grid system,” *Renew. Sustain. Energy Rev.*, vol. 81, no. February 2016, pp. 1329–1349, 2018.

[36] L. De Sousa, B. Silvestre, and B. Bouchez, “A Combined Multiphase Electric Drive and Fast Battery Charger for Electric Vehicles Topology and Electric Propulsion Efficency Analysis,” in *2010 IEEE Vehicle Power and Propulsion Conference*, 2010, pp. 1–6.

[37] D. P. Tuttle and R. Baldick, “The Evolution of Plug-In Electric Vehicle-Grid Interactions,” *IEEE Trans. Smart Grid*, vol. 3, no. 1, pp. 500–505, 2012.

[38] “Electrification of the Transportation System.” MIT Energy Initiative, Cambridge, MA, 2010.

[39] A. Foley, I. Winning, and B. O. Gallachoir, “ELECTRIC VEHICLES: INFRASTRUCTURE REGULATORY REQUIREMENTS,” in *Proceedings of ITRN2010*, 2010, pp. 1–7.

[40] G. Choe, J. Kim, B. Lee, C. Won, and T. Lee, “A Bi-directional Battery Charger for Electric Vehicles Using Photovoltaic PCS Systems,” in *2010 IEEE Vehicle Power and Propulsion Conference*, 2010, pp. 1–6.

[41] F. Musavi, M. Edington, W. Eberle, and W. G. Dunfor, “Evaluation and Efficiency Comparison of Front End AC-DC Plug-in Hybrid Charger Topologies,” *IEEE Trans. Smart Grid*, vol. 3, no. 1, pp. 413–421, 2012.

[42] P. Keil and A. Jossen, “Charging protocols for lithium-ion batteries and their impact

on cycle life-An experimental study with different 18650 high-power cells," *J. Energy Storage*, vol. 6, pp. 125–141, 2016.

[43] T. Kang and B. Chae, "Control Algorithm of Bi-directional Power Flow Rapid Charging System for Electric Vehicle Using Li-Ion Polymer Battery," in *2013 IEEE ECCE Asia Downunder*, 2013, pp. 499–505.

[44] F. Savoye, P. Venet, M. Millet, and J. Groot, "Impact of Periodic Current Pulses on Li-Ion Battery Performance," *IEEE Trans. Ind. Electron.*, vol. 59, no. 9, pp. 3481–3488, 2012.

[45] X. Guo, J. Li, X. Wang, and A. Topology, "Impact of Grid and Load Disturbances on Electric Vehicle Battery in G2V / V2G and V2H Mode," in *2015 IEEE Energy Conversion Congress and Exposition (ECCE)*, 2015, pp. 5406–5410.

[46] J. Y. Yong, S. M. Fazeli, V. K. Ramachandaramurthy, and K. M. Tan, "Design and development of a three-phase off-board electric vehicle charger prototype for power grid voltage regulation," *Energy*, vol. 133, pp. 128–141, 2017.

[47] J. Y. Yong, V. K. Ramachandaramurthy, K. M. Tan, and J. Selvaraj, "Experimental Validation of a Three-Phase Off-Board Electric Vehicle Charger with New Power Grid Voltage Control," *IEEE Trans. Smart Grid*, vol. 9, no. 4, pp. 2703–2713, 2018.

[48] J. W. Kolar and T. Friedli, "The Essence of Three-Phase PFC Rectifier Systems—Part I," *IEEE Trans. POWER Electron.*, vol. 28, no. 1, pp. 176–198, 2013.

[49] J. Dixon, "Three phase Controlled Rectifiers," in *Power Electronic Handbook*, 2010.

[50] A. W. Green, J. T. Boys, and G. F. Gates, "3-phase voltage sourced reversible rectifier," vol. 135, no. 6, 1988.

[51] B. Hauke, "Basic Calculation of a Buck Converter ' s Power Stage," 2015.

[52] K. Colak, E. Asa, and D. Czarkowski, "Dual Closed Loop Control of LLC Resonant Converter for EV Battery Charger," in *International Conference on Renewable Energy*

Research and Applications, 2013, pp. 811–815.

[53] "IEEE Recommended Practice and Requirements for Harmonic Control in Electric Power Systems," *IEEE Power Energy Soc.*, 2014.

[54] H. Saadat, "Symmetrical Components and Unbalanced Fault," in *Power System Analysis*, pp. 400–403.

[55] Y. Tang, C. Luo, J. Yang, and H. He, "A Chance Constrained Optimal Reserve Scheduling Approach for Economic Dispatch Considering Wind Penetration," *IEEE/CAA J. Autom. Sin.*, vol. 4, no. 2, pp. 186–194, 2017.

[56] W. H. Kersting, "Radial Distribution Test Feeders."

[57] "IEEE PES AMPS DSAS Test Feeder Working Group." [Online]. Available: http://sites.ieee.org/pes-testfeeders/resources/.

[58] "Electrical Theory and Practice Tests." [Online]. Available: https://electricalengineeringtutorials.com/effects-of-negative-sequence-currents-in-machines/.

[59] J. Horak, "Zero sequence impedance of overhead transmission lines," in *59th Annual Conference for Protective Relay Engineers, 2006.*, 2006.

[60] H. El-tamaly and H. Ziedan, "Sequence Impedances of Overhead Transmission Lines Carson's Method Versus Rudenberg's Method," in *Proceedings of the 41st International Universities Power Engineering Conference*, 2007.

Appendix A Symmetrical Components

Unbalanced phase quantities such as current and voltage can be replaced by three individual balanced symmetrical components.

A.1 Fundamentals of Symmetrical Components

Consider the phasor representation of a three-phase balanced current shown in (a) (b) (c)

Fig. A.1. Conventionally the direction of the phasors can be considered counterclock-wise. Therefore the three phasors are written as:

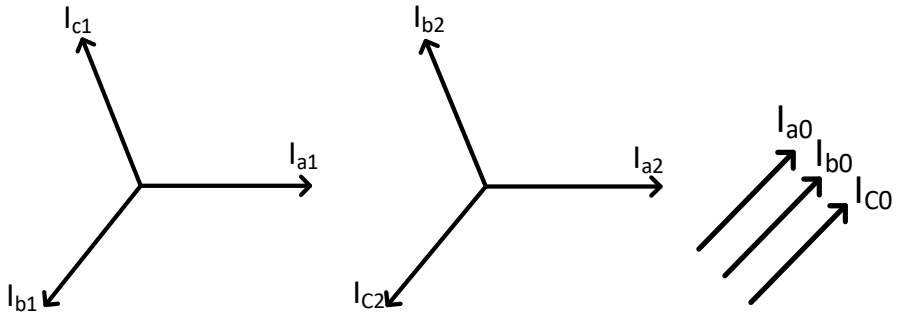

(a) (b) (c)

Fig. A.1 Symmetrical Components.

Therefore, the three phasors are written as:

$$I_{a1} = I_{a1}/\_0 = I_{a1} \tag{A.1}$$

$$I_{b1} = I_{a1}/\_240 = a^2 I_{a1}$$

$$I_{c1} = I_{a1}/\_120 = a I_{a1}$$

Where a is defined as an operator causing 120° counterclock-wise rotation. A is defined as below:

$$a = 1/\_120 = -0.5 + i0.866$$
$$a^2 = I_{a1}/\_240 = -0.5 - i0.866 \quad \text{(A.2)}$$

It is clear that:

$$1 + a + a^2 = 0 \quad \text{(A.3)}$$

The orde of the phasors is abc which is considered as positive sequence but if the order is acb, it will be designated the negative sequence which is equal to the following equation:

$$I_{a2} = I_{a2}/\_0 = I_{a2}$$
$$I_{b2} = I_{a2}/\_120 = a I_{a2} \quad \text{(A.4)}$$
$$I_{c2} = I_{a2}/\_240 = a^2 I_{a2}$$

Another set of balanced phasors is called zero sequence. In this sequence the components are equal in magnitude and they are aligned with each other. The following equation represents zero sequence phasors:

$$I_{a0} = I_{b0} = I_{c0} \quad \text{(A.5)}$$

It is worthy to mention that 0, 1, and 2 are indicating zero, positive, and negative sequence. The symmetrical components were first introduced by C.L. Fortescue in 1918. According to this theory any unbalanced three-phase system can be stated in three balanced system.

In this stage, it is interested to state three-phase currents by symmetrical components. Therefore:

$$I_a = I_{a0} + I_{a1} + I_{a2} \quad \text{(A.6)}$$

$$I_b = I_{b0} + I_{b1} + I_{b2}$$

$$I_c = I_{c0} + I_{c1} + I_{c2}$$

Based on (A. 1), (A. 4), and (A. 5) the previous equation can be written in terms of phase a components:

$$I_a = I_{a0} + I_{a1} + I_{a2}$$

$$I_b = I_{a0} + a^2 I_{a1} + a I_{a2} \tag{A.7}$$

$$I_c = I_{a0} + a I_{a1} + a^2 I_{a2}$$

Or

$$\begin{bmatrix} I_a \\ I_b \\ I_c \end{bmatrix} = \begin{bmatrix} 1 & 1 & 1 \\ 1 & a^2 & a \\ 1 & a & a^2 \end{bmatrix} \begin{bmatrix} I_{a0} \\ I_{a1} \\ I_{a2} \end{bmatrix} \tag{A.8}$$

The above equation can be written as:

$$I^{abc} = A I_a^{012} \tag{A.9}$$

Where A is called transformation matrix transforming phasor currents into symmetrical components, and is:

$$A = \begin{bmatrix} 1 & 1 & 1 \\ 1 & a^2 & a \\ 1 & a & a^2 \end{bmatrix} \tag{A.10}$$

Given I^{abc}, the following equation solves for I_a^{012}:

$$I_a^{012} = A^{-1} I^{abc} \tag{A.11}$$

And

$$A^{-1} = \frac{1}{3} \begin{bmatrix} 1 & 1 & 1 \\ 1 & a & a^2 \\ 1 & a^2 & a \end{bmatrix} \tag{A.12}$$

Substituting for A^{-1} in (A.11):

$$\begin{bmatrix} I_{a0} \\ I_{a1} \\ I_{a2} \end{bmatrix} = \frac{1}{3} \begin{bmatrix} 1 & 1 & 1 \\ 1 & a & a^2 \\ 1 & a^2 & a \end{bmatrix} \begin{bmatrix} I_a \\ I_b \\ I_c \end{bmatrix} \tag{A.13}$$

Thus:

$$I_{a0} = \frac{1}{3}(I_a + I_b + I_c)$$

$$I_{a1} = \frac{1}{3}(I_a + aI_b + a^2 I_c) \quad \text{(A.14)}$$

$$I_{a2} = \frac{1}{3}(I_a + a^2 I_b + aI_c)$$

Similar equations exist for the voltages. Unbalanced phase voltages in terms of the symmetrical components are:

$$V_a = V_{a0} + V_{a1} + V_{a2}$$

$$V_b = V_{a0} + a^2 V_{a1} + aV_{a2} \quad \text{(A.15)}$$

$$V_c = V_{a0} + aV_{a1} + a^2 V_{a2}$$

Symmetrical components in terms of unbalanced voltages are:

$$V_{a0} = \frac{1}{3}(V_a + V_b + V_c)$$

$$V_{a1} = \frac{1}{3}(V_a + aV_b + a^2 V_c) \quad \text{(A.16)}$$

$$V_{a2} = \frac{1}{3}(V_a + a^2 V_b + aV_c)$$

Appendix B

B.1 Newton-Raphson Algorithm

This method is an iterative algorithm based on initial assumption of the unknown variables and use of Taylor's series expansion.

As an example the solution for a one-dimensional equation has been provided bellow:

$$f(x) = c \tag{B.1}$$

Considering $x^{(0)}$ and $\Delta x^{(0)}$ are the initial assumption and deviation from correct answer respectively. Thus:

$$f\left(x^{(0)} + \Delta x^{(0)}\right) = c \tag{B.2}$$

If the left-side of the above equation is expanded by Taylor's series following equation would be the result:

$$f\left(x^{(0)}\right) + \left(\frac{df}{dx}\right)^{(0)} \Delta x^{(0)} + \frac{1}{2!}\left(\frac{d^2 f}{dx^2}\right)^{(0)} (\Delta x^{(0)})^2 + \cdots = c \tag{B.3}$$

If we presume that $\Delta x^{(0)}$ has very small value, the higher order terms are negligible resulting in:

$$\Delta c^{(0)} = \left(\frac{df}{dx}\right)^{(0)} \Delta x^{(0)} \tag{B.4}$$

where

$$\Delta c^{(0)} = c - f\left(x^{(0)}\right) \tag{B.5}$$

By adding $\Delta x^{(0)}$ to $x^{(0)}$, second approximation is calculated and repeating this process results in Newton-Raphson method.

$$\Delta c^{(k)} = c - f\left(x^{(k)}\right) \tag{B.6}$$

$$\Delta x^{(k)} = \frac{\Delta c^{(k)}}{(\frac{df}{dx})^{(k)}} \tag{B.7}$$

$$x^{(k+1)} = x^{(k)} + \Delta x^{(k)} \tag{B.8}$$

Also equation (B. 7) can be written as:

$$\Delta c^{(k)} = \Delta x^{(k)} (\frac{df}{dx})^{(k)} \tag{B.9}$$

Now if we consider n-dimensional function the above mentioned equations are stated in matrices. In this case the Taylor's series would be:

$$(f_1)^{(0)} + (\frac{\partial f_1}{\partial x_1})^{(0)} \Delta x_1{}^{(0)} + \left(\frac{\partial f_1}{\partial x_2}\right)^{(0)} \Delta x_2{}^{(0)} + \cdots + \left(\frac{\partial f_1}{\partial x_n}\right)^{(0)} \Delta x_n{}^{(0)} = c_1$$

$$(f_2)^{(0)} + (\frac{\partial f_2}{\partial x_1})^{(0)} \Delta x_1{}^{(0)} + \left(\frac{\partial f_2}{\partial x_2}\right)^{(0)} \Delta x_2{}^{(0)} + \cdots + \left(\frac{\partial f_2}{\partial x_n}\right)^{(0)} \Delta x_n{}^{(0)} = c_2$$

$$\vdots \tag{B.10}$$

$$(f_n)^{(0)} + (\frac{\partial f_n}{\partial x_1})^{(0)} \Delta x_1{}^{(0)} + \left(\frac{\partial f_n}{\partial x_2}\right)^{(0)} \Delta x_2{}^{(0)} + \cdots + \left(\frac{\partial f_n}{\partial x_n}\right)^{(0)} \Delta x_n{}^{(0)} = c_n$$

In the matrix form

$$\begin{bmatrix} c_1 - (f_1)^{(0)} \\ c_2 - (f_2)^{(0)} \\ \vdots \\ c_n - (f_n)^{(0)} \end{bmatrix} = \begin{bmatrix} (\frac{\partial f_1}{\partial x_1})^{(0)} & \left(\frac{\partial f_1}{\partial x_2}\right)^{(0)} & \cdots & \left(\frac{\partial f_1}{\partial x_n}\right)^{(0)} \\ \left(\frac{\partial f_2}{\partial x_1}\right)^{(0)} & \left(\frac{\partial f_2}{\partial x_2}\right)^{(0)} & \cdots & \left(\frac{\partial f_2}{\partial x_n}\right)^{(0)} \\ \vdots & \vdots & & \\ (\frac{\partial f_n}{\partial x_1})^{(0)} & \left(\frac{\partial f_n}{\partial x_2}\right)^{(0)} & \cdots & \left(\frac{\partial f_n}{\partial x_n}\right)^{(0)} \end{bmatrix} \begin{bmatrix} {\Delta x_1}^{(0)} \\ {\Delta x_2}^{(0)} \\ \vdots \\ {\Delta x_n}^{(0)} \end{bmatrix} \quad \text{(B.11)}$$

The above equation can be summarized as follows:

$$\Delta C^{(k)} = \Delta X^{(k)} (J)^{(k)} \quad \text{(B.12)}$$

Where $(J)^{(k)}$ is called Jacobian matrix, and the elements of this matrix are partial derivatives of n-dimensional functions at $X^{(k)}$.

Finally

$$\Delta X^{(k)} = (J)^{(k)^{-1}} \Delta C^{(k)} \quad \text{(B.13)}$$

$$X^{(k+1)} = \Delta X^{(k)} + X^{(k+1)} \quad \text{(B.14)}$$